



## INTELLIGENT FAULT DIAGNOSIS OF POWER TRANSMISSION LINE USING FUZZY LOGIC AND ARTIFICIAL NEURAL NETWORK

Khaled Omer Mokhtar TOUATI, Mohamed BOUDIAF , Imad MERZOUK , Ahmed HAFIFA

Applied Automation and Industrial Diagnostics Laboratory, Faculty of Sciences and Technology,  
Ziane Achour University, Djelfa, Algeria

\* Corresponding author, e-mail: [boudhiaf\\_mohamed@yahoo.fr](mailto:boudhiaf_mohamed@yahoo.fr)

### Abstract

In the industrial sector, transmission lines are an important part of the electrical grid. Thus it is important to protect it from all the different faults that may occur as soon as possible to supply the electric power continuously. This paper presents a modern solutions and a comparative study of fault detection and identification in electrical transmission lines using artificial neural network (ANN) compare to the fuzzy logic. Faults in transmission line of various types have been created using simulation model. An intelligent monitoring system (IFD: Intelligent Fault Diagnosis) was used at both ends of a 230 kV overhead transmission line, voltage and current measurements exploited as indicator data for this system. Both approaches were found to be robust, accurate and reliable to detect the fault when it occurs, to determine the fault type short circuit or opening of a power line (open circuit), to locate the fault and to determine which phase was faulted.

Keywords: power system diagnosis, fault detection, electrical transmission line, ANN, fuzzy logic.

### ABBREVIATION AND ACRONYMS

$i_{abc}$ : Three-phase currents;  
 $v_{abc}$ : Three-phase voltages;  
 OC: Open Circuit;  
 SC: Short Circuit;  
 ANN: Artificial Neural Network;  
 IFD: Intelligent Fault Diagnosis;  
 $L$ : Inductance,  $C$ : Capacitor,  $R$ : Resistance;  
 $G$ : Ground,  $l$ : Line length;  
 $Ph_i$  and  $i=a,b,c$  Electrical phase;  
 $X$ : Variable;  
 $V_a$ : Electrical voltage amplitude of phase (a);  
 $I_a$ : Electrical current amplitude of phase (a);  
 $m$ : measurement,  $S_b$ : Base power;  
 $Q_k, H_k, L_k, VL_k$  (and  $k=1,2,3\dots$ ): Linguistic variables.

### 1. INTRODUCTION

In power systems, transmission lines play an important role that is transferring electric power from the generating station to load centers, the occurrence of different types of faults on the transmission line is a fact in daily life, although such faults rarely occur and occur at random locations. Therefore, a well-coordinated protection system must be provided to quickly detect and isolate faults, thus minimizing damage to the power system. These faults can be categorized to shunt faults (short-circuit) and series faults (open-circuit) [1], various

possible short circuit faults can be a single phase-ground short-circuit L-G (Pha-gnd, Phb-gnd, Phc-gnd), double phases-ground short-circuit 2L-Gnd (Phab-gnd, Phbc-gnd, Phac-gnd), double phase-ground short-circuit 2L without the ground (Pha-b, Phb-c, Pha-c) and three phases short-circuit 3L (Pha-b-c) with or without the ground [2, 3]. Similarly open circuit faults can be at one phase, two phases or all three phases.

Until now, numerous methods have been conducted to diagnose the transmission lines, these methods can be divided into several categories based on impedance measurement, traveling wave techniques, time domain current & voltage measurements and artificial intelligence.

Several diagnostic techniques are investigated in previous works, as following: Impedance-based methods are mostly divided into two ends methods [4, 5] and one end methods [6, 7], which are considered to be accurate and complete. However, they bring complexity and high computational cost, as some asynchronous methods may have two different results, thus requiring a telecommunications system between the two diagnostic stations and an accurate model of the faulted transmission line. The travelling waves methods based on the high-frequency forward and backward fault signals propagating to both ends along the transmission line, knowing the propagation velocity of waves, the fault location can be calculated after determining the time when these

signals arrive to the ends, these methods can be classified into two ends methods [8, 9], one end methods [10, 11] or both, in [12] a combination of one-end and two-ends techniques is used, although this algorithm accurate and useful to determine the simultaneous faults locations however the obtained accuracy depends on precise synchronization between the two ends which is not economical. In [13], the authors introduced a traveling-wave-based algorithm, this method aims to improve the fault location accuracy by eliminating the synchronization error, yet, in order to realize this method, many measurement devices and satellites are required. A combination of TW and machine learning was introduced in [14], this method has some disadvantages not only it requires a large data and thousands of samples but also the accuracy decreases when the fault is further, in general, these methods have many advantages to summarize: They have a high accuracy, speed and reliability, in addition they are unaffected by load variations or high ground resistance however, the disadvantage of these methods is that they are costly and require high sampling frequencies, some of two ends methods require additional devices or an implemented Global Positioning System (GPS) for synchronizing the signals at both ends [13, 15].

Time domain methods depends on voltages and currents measurements [16, 17]. exploitation of these measurements it varies, in [18] the authors introduce an instantaneous phase angles based-method, that works satisfactorily for high impedance fault and is robust to harmonics however requires a high samplings rate. Another method based on positive sequence superimposed network during auto-reclosing presented in [19] which is reliable and accurate yet the execution time of the proposed method is up to 3 minutes. In [20] Ensemble Kalman Filter presented which is simple method and effective, some other methods rely on transforming signals from time domain to frequency domain such as Wavelet transform [21], FFT [11], S-transform [22] for features extraction from signals that are insufficient and require additional algorithms. However, while achieving satisfactory results, these methods require in-depth knowledge specific to the system configuration.

In recent years, the application of intelligent algorithms has attracted many researchers due to their advantages, in which data are collected under various fault conditions and used to create database and train the algorithms. Comparing the test results with the data base to determine the location and type of fault. In [23] the authors proposed a method based on convolutional neural network (CNN), which is worth investigating due to the large amount of data required and the use of image processing to obtain mainly fault classifications. In the study [24] a neural network model is proposed and used by an automatic learning algorithm. A multi-stage algorithm based on unsupervised feature learning and convolutional sparse Auto encoder was introduced in [25]. A combinations of support vector machines (SVMs)

finite impulse response (FIR) filter and artificial neural network ANN has been proposed in [26]. Fuzzy logic-based methods presented in [27, 28], a combination of fuzzy logic with S-transform [3] and K-Nearest Neighbor Algorithm in [29]. All these algorithms require a large data and some of them reliable for just fault classification.

All of methods above focused on short-circuit faults with no considerations to open-circuit faults. In this work, two advanced algorithms of transmission line fault diagnosis using artificial neural network and fuzzy logic were proposed for the location and classification of short circuit faults, open-circuit faults and the combination of short circuit faults-open circuit faults simultaneously.

Another contribution of this paper is analyzing the implementation of intelligent monitoring methods then comparing their performance, based on fast response times with acceptable delays compared to the opening time of the breaker. The originality and the basic idea of this study is introduced by the detection and identification of all faults types occurring in the electrical transmission network, also the demonstration of the diagnosis robustness for impudent faults or enormous load variations.

## 2. SYSTEM DESCRIPTION

The figure 1 shows a single line diagram of the power system under study which is used to test the intelligent surveillance system. It consists of two electrical sources connected with 200km AC overhead transmission line.

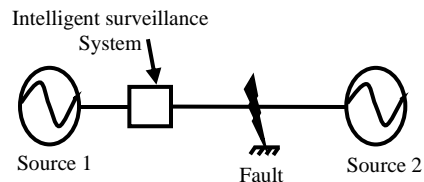


Fig. 1. Power system single line diagram

Figure 2 shows the power system's structure, it consists of a 230kV /50hz source with  $\angle 0^\circ$  phase angel connected to a 230kv/50hz source with  $\angle 27^\circ$  phase angel through an AC overhead transmission line. The distance between the sources is 200 km, it is divided into 4 zones, and each zone is 50 km. The intelligent surveillance system was placed in beginning of the transmission line to measure the currents and voltages ( $I_{123}, V_{123}$ ) after taking the measurements the intelligent system willshows the fault type (short circuit or line drop), the fault zone (1, 2, 3, 4) and the fault phase (1001 means phase A-Ground, 0101 phase B-Ground, 0011....) the full faulted phases will represent later.

The transmission line is represented by a simple circuit ( $\pi$  model) [30], which is composed of a resistor ( $R$ ) and an inductance ( $L$ ) connected in series and a capacitor ( $C$ ) at both ends, as shown in the figure 3.

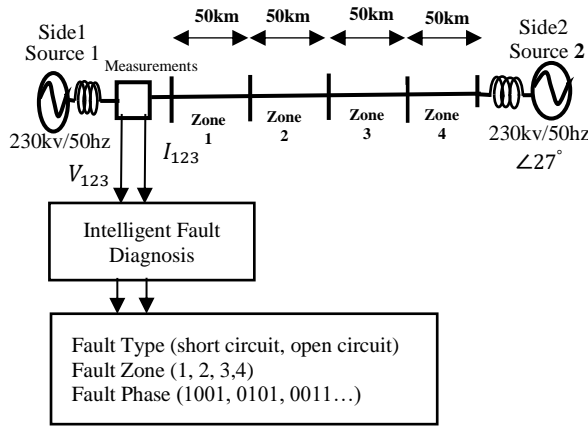


Fig. 2. Diagram of the diagnostic system

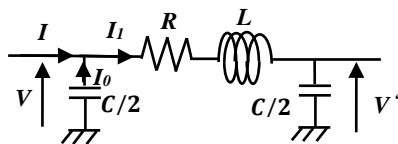


Fig. 3. Line equivalent schematic

From the modeling we obtain:

$$I = I_0 + I_1 \quad \text{and} \quad V - V' = RI_1 + L \frac{dI_1}{dt} \quad (1)$$

From (1), after Laplace Transformation the equations become:

$$I_1 = \frac{V - V'}{R + LS} \quad \text{and} \quad I_0 = \frac{C}{2} \cdot \frac{dV}{dt} \xrightarrow{LT} I_0 = \frac{C}{2} \cdot S \cdot V \quad (2)$$

The cyclic inductance:

$$L = \frac{\mu_0}{2\pi} \left( \frac{\mu_r}{4} + \ln\left(\frac{d_m}{r}\right) \right) \quad (3)$$

The cyclic capacity:

$$C = \frac{2\pi\epsilon_0}{\ln\left(\frac{d_m \cdot 2 \cdot h_m}{r \cdot D_m}\right)} \quad (4)$$

Where:

$d_m$  : Geometric mean distance between phases.

$h_m$  : Geometric mean height of the phases.

$D_m$  : Geometric mean distance between phases and phase images .

$r$ : Conductor diameter,  $\epsilon_0$  : Vacuum dielectric permittivity,  $\mu_0$  : Vacuum magnetic permeability,  $\mu_r$  : Relative magnetic permeability.

The transmission-line parameters:  $Length = 200\text{km}$ ,  $R = 0.103\Omega$  for 1km,  $L = 0.0013\text{H}$  for 1km,  $S_b = 500\text{MVA}$ ,  $C = 8.2 \cdot 10^{-9}$  for 1km,  $U_b = 230 \text{ kV}$ .

### 3. FAULTS TYPES

There are different types of faults in the electrical power system. Our focus in this study is the most common ones: (Short circuit and Open circuit) in transmission line. Figure 4 shows the schematic representation of the faults.

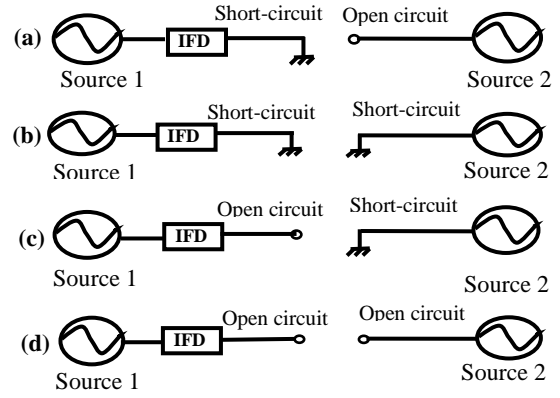


Fig. 4. Faults types

(a) Short circuit to source 1 and open circuit to source 2, (b) Short circuit to both sides, (c) short circuit to source 2 and open circuit to source 1 and (d) open circuit. In all 4 cases the fault type can be a single phase to ground (L-G), two phases (L-L), two phases to ground (2L-G), three phases (3L-G).

In case of an interconnected system we will face a problem which is how to determine if it is a short circuit or open circuit to resolve it we need to use two IFD one at each side like shown in figure 5.

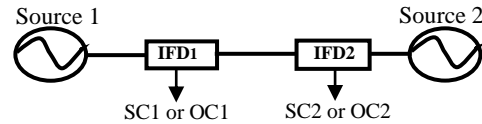


Fig. 5. Dual Surveillance system

### 4. DIAGNOSIS SYSTEM OUTPUT

Figure 6 represents the Diagnosis system outputs, the first output shows the fault type [1 0] indicates the short circuit (SC), [0 1] indicates an open circuit (OC) and [0 0] means there is no fault. The second output shows the location of the fault at which zone (1 to 4). The third output shows which phase is faulted.

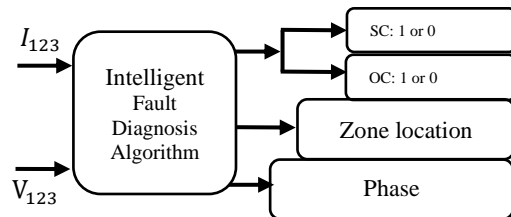


Fig. 6. Diagnosis system output

Table 1 represents all the cases of the fault type (short circuit SC or open circuit OC) to each side's point of view of the intelligent system.

Table 1. Fault type outputs by IFD's

Display	SC		OC	
	side1	side2	side1	side2
sc 1	1	0	0	1
sc 1 & sc2	1	1	0	0
sc 2	0	1	1	0
oc 1 & oc 2	0	0	1	1

**5. DIAGNOSTIC BY THE ARTIFICIAL NEURAL NETWORK ANN**

Figure 7 shows the synoptic diagram of diagnostics by ANN.

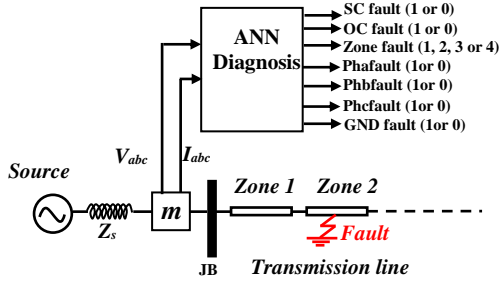


Fig. 7. ANN Diagnosis

Artificial Neural Network (ANN) is a network that uses complex mathematical models for information processing. They are based on functional models of neurons and synapses in the human brain. Similar to the human brain, neural networks connect simple nodes, also called neurons. The collection of these nodes forms a node network, hence the name "neural network". These neurons receive data input and then generates an output by combining the input with its internal activation state and threshold activation function.

A neural network consists of connections, where each connection carries out the output of one neuron, which becomes the input of another neuron in the network. Each connection is assigned a weight, which represents its importance on the neural network. Any neuron can have a relationship with multiple input and output connections [31].

**5.1. Neural network structure**

Neural network has a complex structure composed of artificial neurons, which can receive multiple inputs to generate output, in this study the input layer has six neurons for six inputs the currents magnitudes  $I_1, I_2, I_3$  and the voltages magnitudes  $V_1, V_2, V_3$ . The number of the neurons in the hidden layer and the output layer changes due to outputs as we show next. This network is illustrated in figure 10.

To generate the output signal, the value of  $V$  must be activated with the activation function.

The Logistic Sigmoid or known as binary sigmoid was employed in this study to be the activation function for Hidden layer and the linear activation function is used for the output layer. The error signal is propagated from the output layer to the hidden layer for the  $p$  iteration.

The output value targeted to the  $k$  neuron and the real output obtained by the  $k$  neuron at the output layer [32]. The logistic sigmoid activation function (Log Sigmoid Transfer Function) is:

$$y_j(p) = \frac{1}{1 + e^{-V_j(p)}} \tag{5}$$

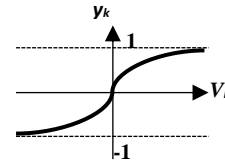


Fig. 8. Log-Sigmoid transfer function

The linear activation function (Pure line Transfer Function) is:

$$y_k = 1 \cdot V_k \tag{6}$$

Fig. 9. Linear transfer function

In this study, the used MLP architecture has been determined as (6, 40, 7). It means the dimensions of the layers are three ( $n=6$ ) input variables, ( $m = 40$ ) nodes in the hidden layer and seven ( $k=7$ ) output nodes, respectively:

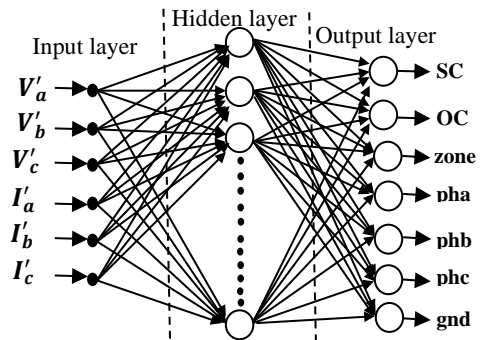


Fig. 10. ANN structure

**5.2. Training algorithms (Levenberg-Marquardt method)**

The Levenberg-Marquardt algorithm was created to approach the second-order training speed without calculating the Hessian matrix. When the performance function has the form of a sum of squares (typical in training feed forward networks).

If  $X_p$  is the  $p^{\text{th}}$  vector comprised of weight value and threshold value, then  $X_{p+1}$  is calculated from:

$$X_{p+1} = X_p + \Delta X, \quad X_{p+1} = W_{p+1} + \Delta X, \quad X_{p+1} = W_p \tag{7}$$

According to newton algorithm,  $\Delta X$  is given by:

$$\Delta X = -[\nabla^2 E(x)]^{-1} \nabla E(x) \tag{8}$$

Then the Hessian matrix can be approximated as:

$$H = J^T J \tag{9}$$

Where  $\nabla^2 E(x)$  is the hessian matrix of error indicator function  $E(x)$ .  $\nabla E(x)$  is the gradient We define  $E(x)$  by the following equation:

$$E(x) = (\frac{1}{2}) \sum_{i=1}^N e_i^2(x) \tag{10}$$

Where  $e(x)$  is the training error.

$\nabla E(x)$  and  $\nabla^2 E(x)$  are calculated from Eq (11) and (12) respectively:

$$\nabla E(x) = J^T(x)e(x) \tag{11}$$

$$\nabla^2 E(x) = J^T(x)e(x) + S(x) \tag{12}$$

Where  $S(x) = \sum_{i=1}^N e_i(x) \nabla^2 e_i(x)$ .  $J(x)$  is the jacobian matrix given by:

$$J(x) = \begin{bmatrix} \frac{\partial e_1(x)}{\partial x_1} & \frac{\partial e_1(x)}{\partial x_2} & \dots & \frac{\partial e_1(x)}{\partial x_n} \\ \frac{\partial e_2(x)}{\partial x_1} & \frac{\partial e_2(x)}{\partial x_2} & \dots & \frac{\partial e_2(x)}{\partial x_n} \\ \dots & \dots & \dots & \dots \\ \frac{\partial e_n(x)}{\partial x_1} & \frac{\partial e_n(x)}{\partial x_2} & \dots & \frac{\partial e_n(x)}{\partial x_n} \end{bmatrix} \tag{13}$$

According to gauss-newton algorithm,  $\Delta X$  can be written as follows:

$$\Delta X = -[J^T(x)J(x)]^{-1} J(x)e(x) \tag{14}$$

Meanwhile, according to LM algorithm  $\Delta X$  can be rewritten as follows:

$$\Delta X = -[J^T(x)J(x) + \mu I]^{-1} J(x)e(x) \tag{15}$$

and the gradient can be computed as:

$$g = J^T e \tag{16}$$

Where  $J$  is the Jacobian matrix, which contains the first derivative of the network error with respect to the weight and bias, and  $(e(x))$ : Training error) is the network error vector. The Jacobian matrix can be calculated by the standard back propagation technique, which is much simpler than calculating the Hessian matrix. The Levenberg-Marquardt algorithm uses this approximation to the Hessian matrix in the following Newton-like updates:

$$X_{p+1} = x_k - [H + \mu I]^{-1} \cdot g \tag{17}$$

$$X_{p+1} = x_k - [J^T J + \mu I]^{-1} \cdot J^T e \tag{18}$$

When the scalar  $\mu$  is zero, this is just Newton's method, using an approximate Hessian matrix. When  $\mu$  is larger, this becomes a gradient descent with a smaller step size. Newton's method is faster and more accurate near the minimum error, so the goal is to switch to Newton's method as soon as possible. Therefore, after each successful step (decrease of the performance function),  $\mu$  will decrease and increase only when the tentative step increases the performance function. In this way, in each iteration of the algorithm the performance function is always reduced [33, 34].

### 5.3. Training base

#### 5.3.1. Adaptation of measurements with neural network input

To reduce the complexity of the neural network and to process all possible values, we can specify as inputs the numbering of the variation intervals for the quantities to be measured like represented in table 2 ( $I_a$  is an example, all the currents  $I_a, I_b, I_c$  magnitudes and voltages  $V_a, V_b, V_c$  magnitudes were used), this method has the advantage that is covering all the zone from  $1km$  to  $50km$  thus doesn't mix between the zones when the fault occurs on the zone's boundaries and covers a large range of fault resistance.

Table. 2. Variation intervals as ANN inputs

Size measured	Variation interval	Interval numbering (specification of neural network inputs)
$I_a (pu)$	$I_a \leq 0.015$	1
	$0.015 < I_a \leq 0.03$	2
	$0.03 < I_a \leq 0.045$	3
	$0.045 < I_a \leq 0.1$	4
	$0.1 < I_a \leq 0.6$	5
	$0.6 < I_a \leq 1.27$	6
	$1.27 < I_a \leq 1.71$	7
	$1.71 < I_a \leq 2.61$	8
	$2.61 < I_a \leq 9$	9
$V_a (pu)$	$V_a \leq 0.53$	1
	$0.53 < V_a \leq 0.7$	2
	$0.7 < V_a \leq 0.78$	3
	$0.78 < V_a \leq 0.85$	4
	$0.85 < V_a \leq 5$	5

#### 5.3.2. Training table

The following table 3 presents all the training data for ANN.

## 6. DIAGNOSTIC BY FUZZY LOGIC METHOD

Figure 11 represents the implantation of the fuzzy logic diagnosis system at the beginning of the transmission line. As we shown earlier that one IFD isn't enough and it has to add another IFD at the other end of the transmission line like in figure 12.

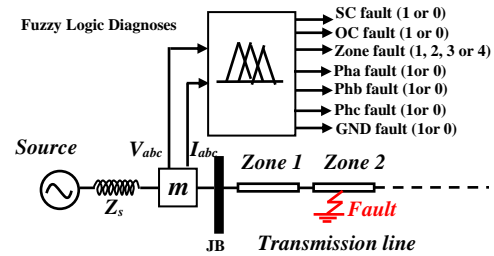


Fig. 11. Fuzzy logic implantation

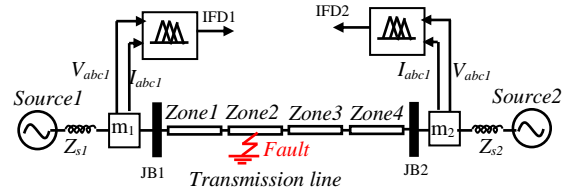


Fig. 12. Fuzzy logic implantation at both ends.

### 6.1. Bloc diagram of fuzzy logic

A simple overall organization of a fuzzy scheme consists of fuzzification, fuzzy inference system, fuzzy rule base and defuzzification as displayed in Figure 13 for fault identification and localization: In into a fuzzy set. Then, the fuzzy rule base makes it

Table 3. Training Values

No	$i_a$	$i_b$	$i_c$	$V_a$	$V_b$	$V_c$	SC	OC	Zone	Ph <sub>a</sub>	Ph <sub>b</sub>	Ph <sub>c</sub>	GND
1	5	5	5	5	5	5	0	0	0	0	0	0	0
2	9	5	5	1	5	5	1	0	1	1	0	0	1
3	5	9	5	5	1	5	1	0	1	0	1	0	1
4	5	5	9	5	5	1	1	0	1	0	0	1	1
5	9	9	5	1	1	5	1	0	1	1	1	0	1
6	9	9	5	2	1	5	1	0	1	1	1	0	0
7	5	9	9	5	1	1	1	0	1	0	1	1	1
8	5	9	9	5	2	1	1	0	1	0	1	1	0
9	9	5	9	1	5	1	1	0	1	1	0	1	1
10	9	5	9	1	5	2	1	0	1	1	0	1	0
11	9	9	9	1	1	1	1	0	1	1	1	1	1
12	1	5	5	5	5	5	0	1	1	1	0	0	0
13	5	1	5	5	5	5	0	1	1	0	1	0	0
14	5	5	1	5	5	5	0	1	1	0	0	1	0
15	1	1	5	5	5	5	0	1	1	1	1	0	0
16	5	1	1	5	5	5	0	1	1	0	1	1	0
17	1	5	1	5	5	5	0	1	1	1	0	1	0
18	1	1	1	5	5	5	0	1	1	1	1	1	0
19	8	5	5	2	5	5	1	0	2	1	0	0	1
20	5	8	5	5	2	5	1	0	2	0	1	0	1
21	5	5	8	5	5	2	1	0	2	0	0	1	1
22	8	8	5	2	2	5	1	0	2	1	1	0	1
23	7	8	5	4	2	5	1	0	2	1	1	0	0
24	5	8	8	5	2	2	1	0	2	0	1	1	1
25	5	7	8	5	4	2	1	0	2	0	1	1	0
26	8	5	8	2	5	2	1	0	2	1	0	1	1
27	8	5	7	2	5	4	1	0	2	1	0	1	0
28	8	8	8	2	2	2	1	0	2	1	1	1	1
29	2	5	5	5	5	5	0	1	2	1	0	0	0
30	5	2	5	5	5	5	0	1	2	0	1	0	0
31	5	5	2	5	5	5	0	1	2	0	0	1	0
32	2	2	5	5	5	5	0	1	2	1	1	0	0
33	5	2	2	5	5	5	0	1	2	0	1	1	0
34	2	5	2	5	5	5	0	1	2	1	0	1	0
35	2	2	2	5	5	5	0	1	2	1	1	1	0
36	7	5	5	3	5	5	1	0	3	1	0	0	1
37	5	7	5	5	3	5	1	0	3	0	1	0	1
38	5	5	7	5	5	3	1	0	3	0	0	1	1
39	7	7	5	3	3	5	1	0	3	1	1	0	1
40	6	7	5	5	3	5	1	0	3	1	1	0	0
41	5	7	7	5	3	3	1	0	3	0	1	1	1
42	5	6	7	5	5	3	1	0	3	0	1	1	0
43	7	5	7	3	5	3	1	0	3	1	0	1	1
44	7	5	6	3	5	5	1	0	3	1	0	1	0
45	7	7	7	3	3	3	1	0	3	1	1	1	1
46	3	5	5	5	5	5	0	1	3	1	0	0	0
47	5	3	5	5	5	5	0	1	3	0	1	0	0
48	5	5	3	5	5	5	0	1	3	0	0	1	0
49	3	3	5	5	5	5	0	1	3	1	1	0	0
50	5	3	3	5	5	5	0	1	3	0	1	1	0
51	3	5	3	5	5	5	0	1	3	1	0	1	0
52	3	3	3	5	5	5	0	1	3	1	1	1	0
53	6	5	5	4	5	5	1	0	4	1	0	0	1
54	5	6	5	5	4	5	1	0	4	0	1	0	1
55	5	5	6	5	5	4	1	0	4	0	0	1	1
56	6	6	5	4	4	5	1	0	4	1	1	0	1
57	6	6	5	5	4	5	1	0	4	1	1	0	0
58	5	6	6	5	4	4	1	0	4	0	1	1	1
59	5	6	6	5	5	4	1	0	4	0	1	1	0
60	6	5	6	4	5	4	1	0	4	1	0	1	1
61	6	5	6	4	5	5	1	0	4	1	0	1	0
62	6	6	6	4	4	4	1	0	4	1	1	1	1
63	4	5	5	5	5	5	0	1	4	1	0	0	0
64	5	4	5	5	5	5	0	1	4	0	1	0	0
65	5	5	4	5	5	5	0	1	4	0	0	1	0
66	4	4	5	5	5	5	0	1	4	1	1	0	0
67	5	4	4	5	5	5	0	1	4	0	1	1	0
68	4	5	4	5	5	5	0	1	4	1	0	1	0
69	4	4	4	5	5	5	0	1	4	1	1	1	0

the fuzzification stage, the input signals are mapped possible to decide the type of defect. Finally, in the defuzzification step, the fuzzy output set is mapped to the defect type [35].

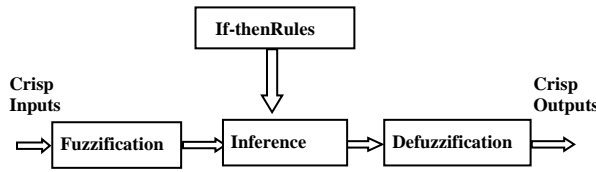


Fig. 13. Block diagram of fuzzy logic

**6.2. Fuzzification**

It is the process of using the information in the knowledge base to convert crisp input values into fuzzy values. Although various types of curves can be used, Gauss, triangles and trapezoids are the most commonly used in fuzzification process.

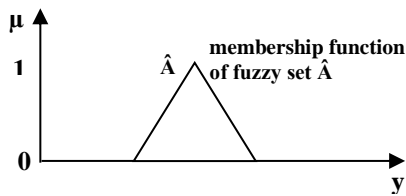


Fig. 14. Membership function

The triangular type was used in our case. Where  $I_a, I_b, I_c, V_a, V_b, V_c$  values were converted to a fuzzy values (very low, low, high) as represented in figure 15. And, the fuzzification of the outputs is represented in figure 16.

**6.3. Rule base**

In this step, the Rule base is formulated as a finite number of rules. The rule base contains the rules that are to be used in making decisions. These rules are generally based on personal experience and intuition. A rule is composed of two main parts: an antecedent block (between the If and Then) and a consequent block (following Then). If (antecedent) Then (consequent) Like in our case if  $I_a, I_b, I_c,$  are high and  $V_a, V_b, V_c$  are low then the system is clear and there is no fault. All the rules are shown in table 4.

**6.4. Inference**

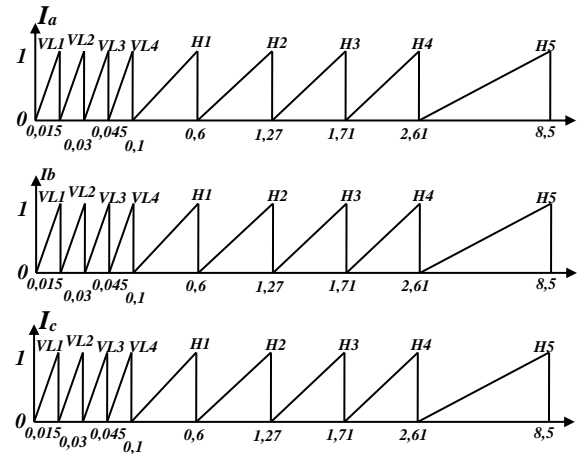
Fuzzy decisions are produced in this process using the rules in the rule base. During this process, each rule is evaluated separately and then a decision is made for each individual rule. The result is a set of fuzzy decisions. Logical operators, such as “AND,” “OR,” and “NOT” define how the fuzzy variables are combined.

**6.5. Defuzzification**

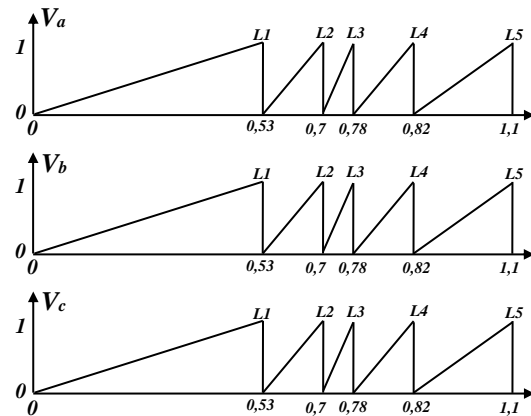
Compared with the fuzzification process, defuzzification is an inverse transformation, because in this process, the fuzzy output is converted into a crisp value and applied to the system. In our application, we use the centroid method:

$$U_{out} = \frac{\sum_{i=1}^n h_i u_i}{\sum_{i=1}^n u_i} \tag{19}$$

$u_i$  is the membership function and  $h_i$  is its center.



(a) Fuzzification current ( $I_a, I_b,$  and  $I_c$ )



(b) Fuzzification Voltage ( $V_a, V_b,$  and  $V_c$ )

Fig. 15. Fuzzification Inputs

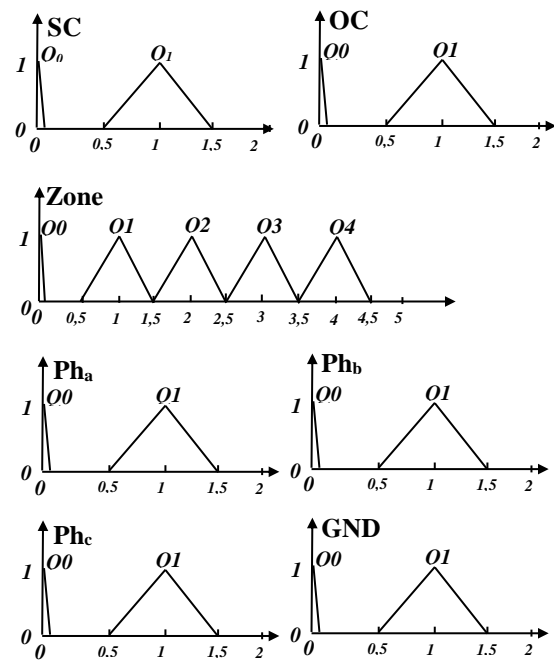


Fig. 16. Fuzzification Outputs

Table 4. Inferences Rules

No	$i_a$	$i_b$	$i_c$	$V_a$	$V_b$	$V_c$	SC	OC	Zone	Ph <sub>a</sub>	Ph <sub>b</sub>	Ph <sub>c</sub>	GND
1	H1	H1	H1	L5	L5	L5	Q0	Q0	Q0	Q0	Q0	Q0	Q0
2	H5	H1	H1	L1	L5	L5	Q1	Q0	Q1	Q1	Q0	Q0	Q1
3	H1	H5	H1	L5	L1	L5	Q1	Q0	Q1	Q0	Q1	Q0	Q1
4	H1	H1	H5	L5	L5	L1	Q1	Q0	Q1	Q0	Q0	Q1	Q1
5	H5	H5	H1	L1	L1	L5	Q1	Q0	Q1	Q1	Q1	Q0	Q1
6	H5	H5	H1	L2	L1	L5	Q1	Q0	Q1	Q1	Q1	Q0	Q0
7	H1	H5	H5	L5	L1	L1	Q1	Q0	Q1	Q0	Q1	Q1	Q1
8	H1	H5	H5	L5	L2	L1	Q1	Q0	Q1	Q0	Q1	Q1	Q0
9	H5	H1	H5	L1	L5	L1	Q1	Q0	Q1	Q1	Q0	Q1	Q1
10	H5	H1	H5	L1	L5	L2	Q1	Q0	Q1	Q1	Q0	Q1	Q0
11	H5	H5	H5	L1	L1	L1	Q1	Q0	Q1	Q1	Q1	Q1	Q1
12	VL1	H1	H1	L5	L5	L5	Q0	Q1	Q1	Q1	Q0	Q0	Q0
13	H1	VL1	H1	L5	L5	L5	Q0	Q1	Q1	Q0	Q1	Q0	Q0
14	H1	H1	VL1	L5	L5	L5	Q0	Q1	Q1	Q0	Q0	Q1	Q0
15	VL1	VL1	H1	L5	L5	L5	Q0	Q1	Q1	Q1	Q1	Q0	Q0
16	H1	VL1	VL1	L5	L5	L5	Q0	Q1	Q1	Q0	Q1	Q1	Q0
17	VL1	H1	VL1	L5	L5	L5	Q0	Q1	Q1	Q1	Q0	Q1	Q0
18	VL1	VL1	VL1	L5	L5	L5	Q0	Q1	Q1	Q1	Q1	Q1	Q0
19	H4	H1	H1	L2	L5	L5	Q1	Q0	Q2	Q1	Q0	Q0	Q1
20	H1	H4	H1	L5	L2	L5	Q1	Q0	Q2	Q0	Q1	Q0	Q1
21	H1	H1	H4	L5	L5	L2	Q1	Q0	Q2	Q0	Q0	Q1	Q1
22	H4	H4	H1	L2	L2	L5	Q1	Q0	Q2	Q1	Q1	Q0	Q1
23	H3	H4	H1	L4	L2	L5	Q1	Q0	Q2	Q1	L1	Q0	Q0
24	H1	H4	H4	L5	L2	L2	Q1	Q0	Q2	Q0	Q1	Q1	Q1
25	H1	H3	H4	L5	L4	L2	Q1	Q0	Q2	Q0	Q1	Q1	Q0
26	H4	H1	H4	L2	L5	L2	Q1	Q0	Q2	Q1	Q0	Q1	Q1
27	H4	H1	H3	L2	L5	L4	Q1	Q0	Q2	Q1	Q0	Q1	Q0
28	H4	H4	H4	L2	L2	L2	Q1	Q0	Q2	Q1	Q1	Q1	Q1
29	VL2	H1	H1	L5	L5	L5	Q0	Q1	Q2	Q1	Q0	Q0	Q0
30	H1	VL2	H1	L5	L5	L5	Q0	Q1	Q2	Q0	Q1	Q0	Q0
31	H1	H1	VL2	L5	L5	L5	Q0	Q1	Q2	Q0	Q0	Q1	Q0
32	VL2	VL2	H1	L5	L5	L5	Q0	Q1	Q2	Q1	Q1	Q0	Q0
33	H1	VL2	VL2	L5	L5	L5	Q0	Q1	Q2	Q0	Q1	Q1	Q0
34	VL2	H1	VL2	L5	L5	L5	Q0	Q1	Q2	Q1	Q0	Q1	Q0
35	VL2	VL2	VL2	L5	L5	L5	Q0	Q1	Q2	Q1	Q1	Q1	Q0
36	H3	H1	H1	L3	L5	L5	Q1	Q0	Q3	Q1	Q0	Q0	Q1
37	H1	H3	H1	L5	L3	L5	Q1	Q0	Q3	Q0	Q1	Q0	Q1
38	H1	H1	H3	L5	L5	L3	Q1	Q0	Q3	Q0	Q0	Q1	Q1
39	H3	H3	H1	L3	L3	L5	Q1	Q0	Q3	Q1	Q1	Q0	Q1
40	H2	H3	H1	L5	L3	L5	Q1	Q0	Q3	Q1	Q1	Q0	Q0
41	H1	H3	H3	L5	L3	L3	Q1	Q0	Q3	Q0	Q1	Q1	Q1
42	H1	H2	H3	L5	L5	L3	Q1	Q0	Q3	Q0	Q1	Q1	Q0
43	H3	H1	H3	L3	L5	L3	Q1	Q0	Q3	Q1	Q0	Q1	Q1
44	H3	H1	H2	L3	L5	L5	Q1	Q0	Q3	Q1	Q0	Q1	Q0
45	H3	H3	H3	L3	L3	L3	Q1	Q0	Q3	Q1	Q1	Q1	Q1
46	VL3	H1	H1	L5	L5	L5	Q0	Q1	Q3	Q1	Q0	Q0	Q0
47	H1	VL3	H1	L5	L5	L5	Q0	Q1	Q3	Q0	Q1	Q0	Q0
48	H1	H1	VL3	L5	L5	L5	Q0	Q1	Q3	Q0	Q0	Q1	Q0
49	VL3	VL3	H1	L5	L5	L5	Q0	Q1	Q3	Q1	Q1	Q0	Q0
50	H1	VL3	VL3	L5	L5	L5	Q0	Q1	Q3	Q0	Q1	Q1	Q0
51	VL3	H1	VL3	L5	L5	L5	Q0	Q1	Q3	Q1	Q0	Q1	Q0
52	VL3	VL3	VL3	L5	L5	L5	Q0	Q1	Q3	Q1	Q1	Q1	Q0
53	H2	H1	H1	L4	L5	L5	Q1	Q0	Q4	Q1	Q0	Q0	Q1
54	H1	H2	H1	L5	L4	L5	Q1	Q0	Q4	Q0	Q1	Q0	Q1
55	H1	H1	H2	L5	L5	L4	Q1	Q0	Q4	Q0	Q0	Q1	Q1
56	H2	H2	H1	L4	L4	L5	Q1	Q0	Q4	Q1	Q1	Q0	Q1
57	H2	H2	H1	L5	L4	L5	Q1	Q0	Q4	Q1	Q1	Q0	Q0
58	H1	H2	H2	L5	L4	L4	Q1	Q0	Q4	Q0	Q1	Q1	Q1
59	H1	H2	H2	L5	L5	L4	Q1	Q0	Q4	Q0	Q1	Q1	Q0
60	H2	H1	H2	L4	L5	L4	Q1	Q0	Q4	Q1	Q0	Q1	Q1
61	H2	H1	H2	L4	L5	L5	Q1	Q0	Q4	Q1	Q0	Q1	Q0
62	H2	H2	H2	L4	L4	L4	Q1	Q0	Q4	Q1	Q1	Q1	Q1
63	VL4	H1	H1	L5	L5	L5	Q0	Q1	Q4	Q1	Q0	Q0	Q0
64	H1	VL4	H1	L5	L5	L5	Q0	Q1	Q4	Q0	Q1	Q0	Q0
65	H1	H1	VL4	L5	L5	L5	Q0	Q1	Q4	Q0	Q0	Q1	Q0
66	VL4	VL4	H1	L5	L5	L5	Q0	Q1	Q4	Q1	Q1	Q0	Q0
67	H1	VL4	VL4	L5	L5	L5	Q0	Q1	Q4	Q0	Q1	Q1	Q0
68	VL4	H1	VL4	L5	L5	L5	Q0	Q1	Q4	Q1	Q0	Q1	Q0
69	VL4	VL4	VL4	L5	L5	L5	Q0	Q1	Q4	Q1	Q1	Q1	Q0

## 7. SIMULATION RESULTS

This section presents the tests results of different faults on the transmission line to illustrate the reliability, the robustness and the response time of the IFD's systems, using ANN and FL algorithms. The diagnostic systems used are capable of detecting (69 x 2 = 138) types of faults. Considering the tripping time of the protection equal to 200 msec.

### 7.1. Diagnostic performances

To test the performance of both diagnostic approaches, several types of fault are presented (SC: Short-Circuit or OC: Open Circuit). For each case, the variation of the three-phase currents and voltages in the two sides of the electrical line, the indication of the fault zone in the two sides of IFD, the fault type indication (SC or OC) and the fault phase identification (pha, phb, phc, GND) are studied. Every fault for all cases occurs at 0,1sec.

In the 1<sup>st</sup> case, the appearance of a single-phase fault in the 1<sup>st</sup> Zone is applied in 4 different types:

- SC Phase a - GND (both sides),
- SC Phase a - GND (Side 1),
- SC Phase a - GND (Side 2),
- OC Phase a.

Figures 17-24 show the results and the response of each IFD in the event of a single-phase short circuit fault SC Ph<sub>a</sub>-GND occurring in the electrical line. Figures 17 and 18 show the transient behavior of three-phase currents and voltages in both sides.

Can be notice:

- A large decrease in voltage and a large increase in current (of phase a) on side 1.
- A slight decrease in voltage and a large increase in current (of phase a) on side 2.

According to fuzzy logic, the fault zone represented as zone 1 to the IFD1 point of view and zone 4 to the IFD2 (Fig. 19). To both IFD systems this fault is a short-circuit (SC) as shown (Fig. 20). In Figure 21, fuzzy logic identifies the fault in phase (a) shorted to ground in both IFD systems. Figures 22-24 show the performance of fault signalization by artificial neural networks. The same representation as the fuzzy logic earlier starting with fault zone (location) then the fault type to both IFD systems (short-circuit or open circuit) and the fault classification (the faulted phases).

By using both intelligent diagnostic methods, the same signature of detection, identification and location of the fault is obtained. In both cases, fault signalization has been shown to be correct after small shifts and considerable transitional regime due to the random evolution of currents and voltages in both sides of the line.

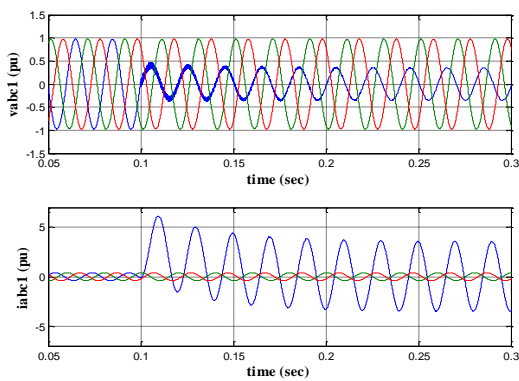


Fig. 17.  $v_{abc1}$  and  $i_{abc1}$  with SC fault of Ph<sub>a</sub>-GND

Figures 25-32 show the diagnosis performance of each IFD when applying a single-phase short circuit fault SC Ph<sub>a</sub>-GND – Side 1.

In figures 25 and 26, can be notice:

- A significant increase in current and a decrease in voltage in phase a (side 1) during the fault.
- Also, a low current and a slight transient voltage variation (in phase a) on side 2.

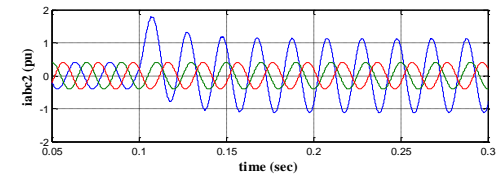
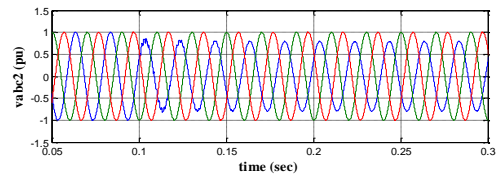


Fig. 18.  $v_{abc2}$  and  $i_{abc2}$  with SC fault of Ph<sub>a</sub>-GND

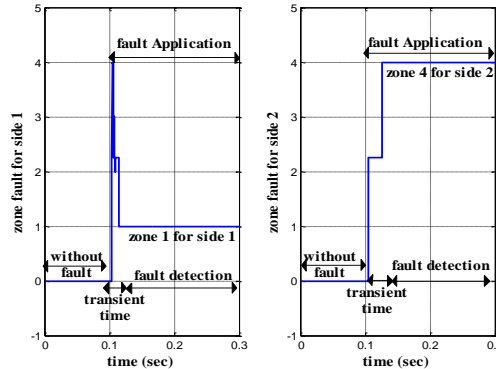


Fig. 19. Fault zone detection for SC Ph<sub>a</sub>-GND (by fuzzy logic)

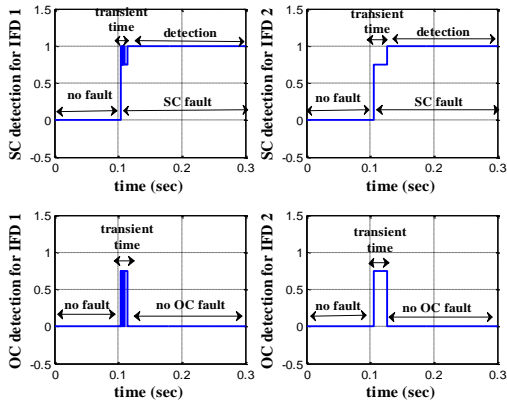


Fig. 20. Fault type identification for SC-Side1 and SC-Side2 (by fuzzy logic)

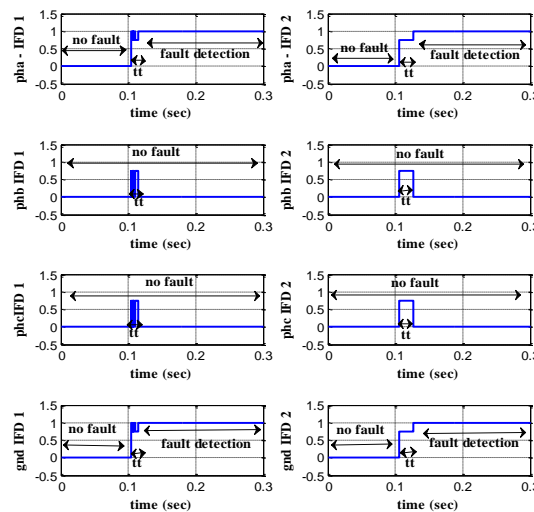


Fig. 21. Fault phase identification Ph<sub>a</sub>-GND (by fuzzy logic)

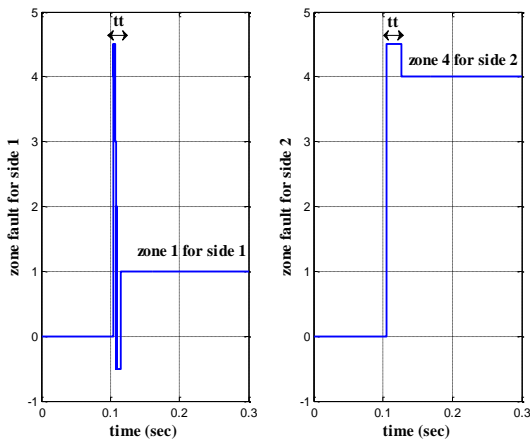


Fig. 22. Fault zone detection for SC Ph<sub>a</sub>-GND (by neural networks)

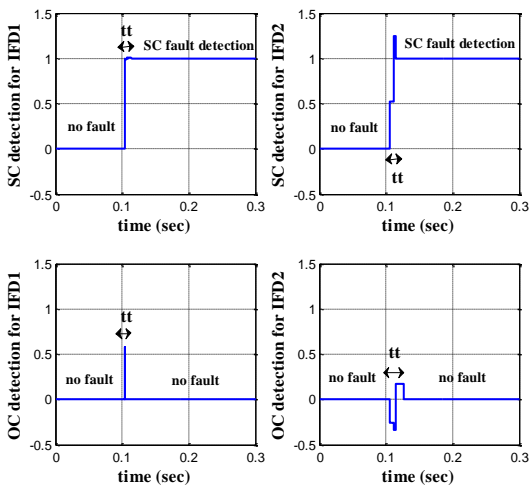


Fig. 23. Fault type identification for SC-Side1 and SC-Side2 (by neural networks)

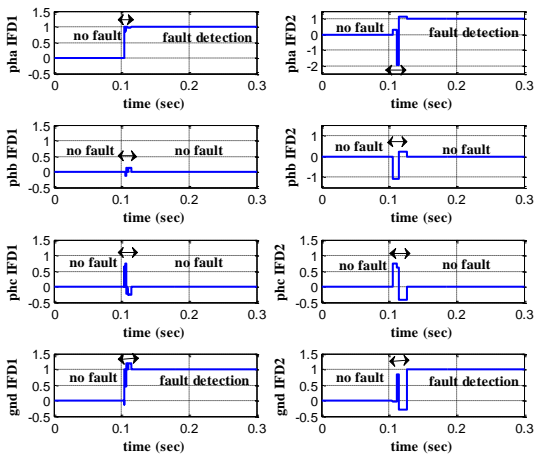


Figure. 24. Fault phase identification Ph<sub>a</sub>-GND (by neural networks)

Using fuzzy logic makes it possible to obtain the performances like shown in figures 27, 28 and 29 below: The results prove the correct signalization of the fault zone with a small delay at IFD2 (side 2) and a small transient regime at IFD1 (side 1) due to the transient evolution lasting time 20msec which is much less than 200 msec (the protection tripping

time). In the same way, Figures 27 and 28 successively show the identification of the fault type and the fault phase: A short circuit with respect to IFD1 (Side 1), an opening of circuit with respect to IFD2 (Side 2) and a fault signaling on phase a.

Using the neural network, also the determination of the fault location is correct, type identification and fault phase identically with fuzzy logic (Figs. 30, 31 and 32). Always there are fast shifts or transients due to random disturbance of current and voltage in both sides of the power line.

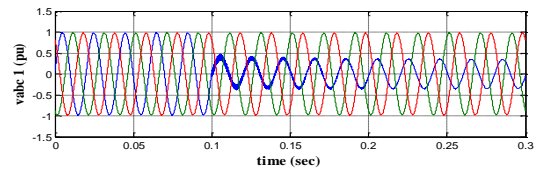


Fig. 25.  $v_{abc1}$  and  $i_{abc1}$  with SC fault of Ph<sub>a</sub>-GND-Side1

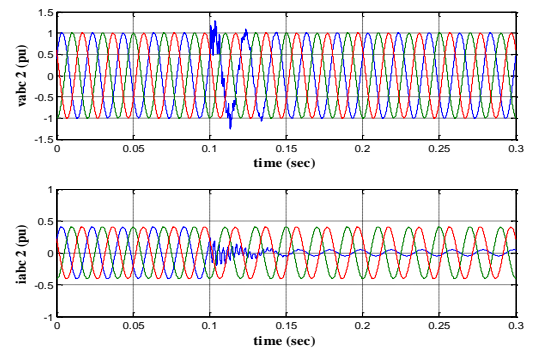


Fig. 26.  $v_{abc2}$  and  $i_{abc2}$  with SC fault of Ph<sub>a</sub>-GND-Side1

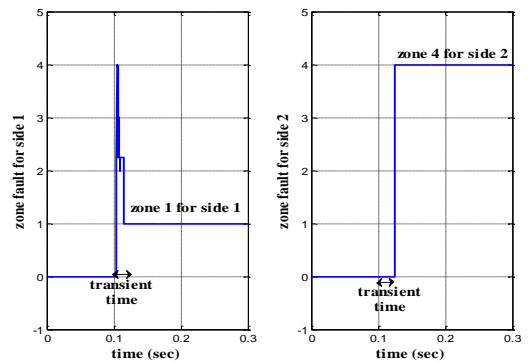


Fig. 27. Fault zone detection for SC Ph<sub>a</sub>-GND-Side1 (by fuzzy logic)

Figures 33-40 show the diagnosis performance of each IFD when applying a single-phase short circuit fault SC Ph<sub>a</sub>-GND – Side 2.

In this case, a short circuit fault to side 2 of the power line. There is a small transient voltage disturbance and a cancellation of the current on phase (a) at side 01. And, a significant increase in current with a slight decrease in voltage on phase (a) at side 02 (Figs. 33 and 34).

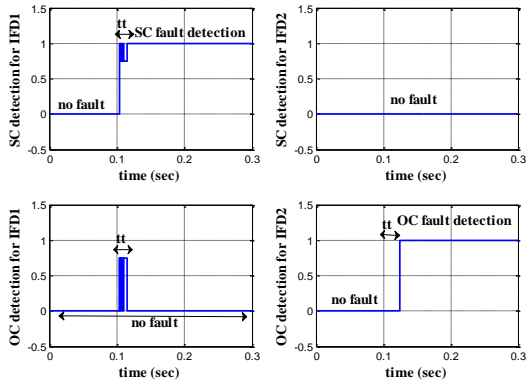


Fig. 28. Fault type identification for SC-Side1 and OC-Side2 (by fuzzy logic)

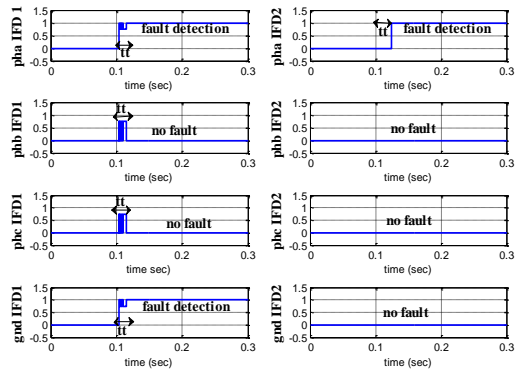


Fig. 29. Fault phase identification  $Ph_a$ -GND-Side1 (by fuzzy logic)

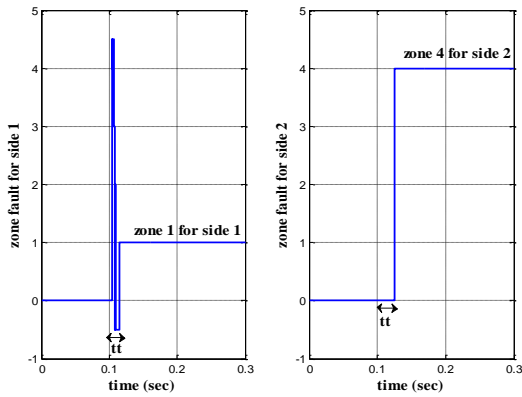


Fig. 30. Fault zone detection for SC  $Ph_a$ -GND-Side1 (by neural networks)

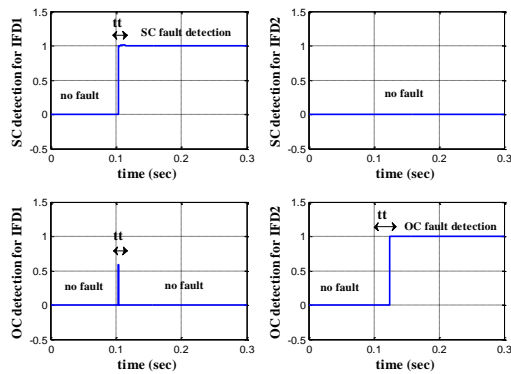


Fig. 31. Fault type identification for SC-Side1 and OC-Side2 (by neural networks)

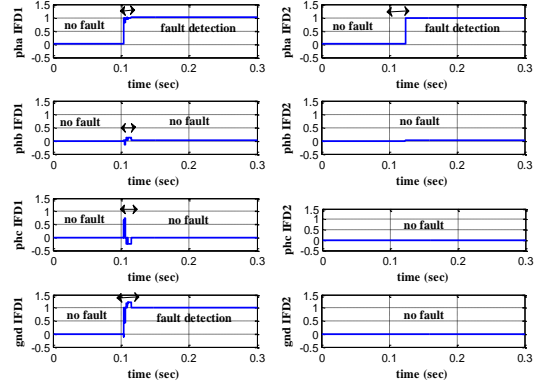


Fig. 32. Fault phase identification  $Ph_a$ -GND-Side1 (by neural networks)

The implementation of two diagnostic methods (fuzzy logic and neural network) makes it possible to locate and identify the fault correctly with small fast transient variations: The fault in zone 1 compared to IFD1 and is a short-circuit on phase (a) at side 2 (Figs 35, 36, 37, 38, 39 and 40).

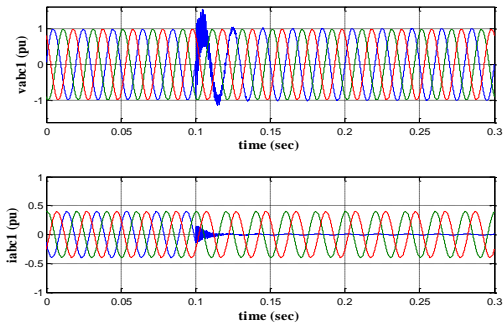


Fig. 33.  $v_{abc1}$  and  $i_{abc1}$  with SC fault of  $Ph_a$ -GND-Side2

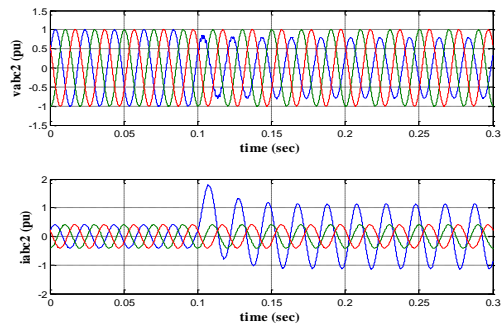


Fig. 34.  $v_{abc2}$  and  $i_{abc2}$  with SC fault of  $Ph_a$ -GND-Side2

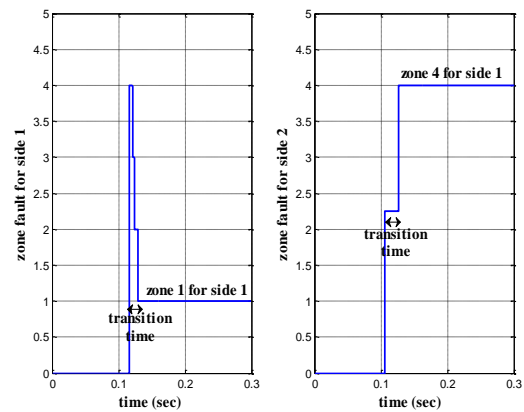


Fig. 35. Fault zone detection for SC  $Ph_a$ -GND-Side2 (by fuzzy logic)

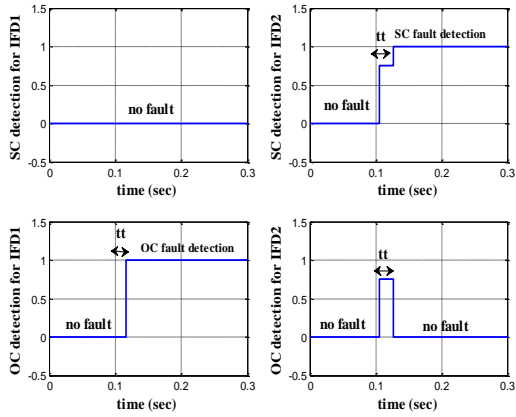


Figure. 36. Fault type identification for OC-Side1 and SC-Side2 (by fuzzy logic)

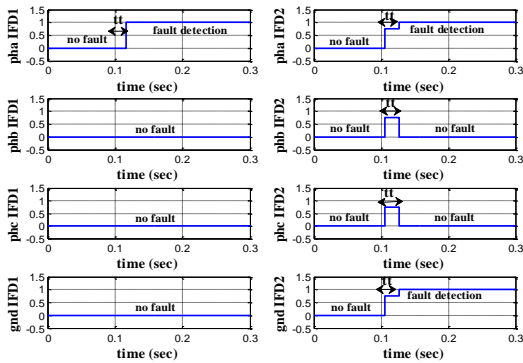


Fig. 37. Fault phase identification  $Ph_a$ -GND-Side2 (by fuzzy logic)

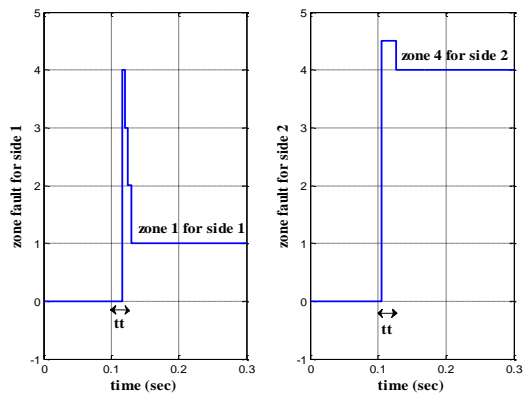


Fig. 38. Fault zone detection for SC  $Ph_a$ -GND-Side2 (by neural networks)

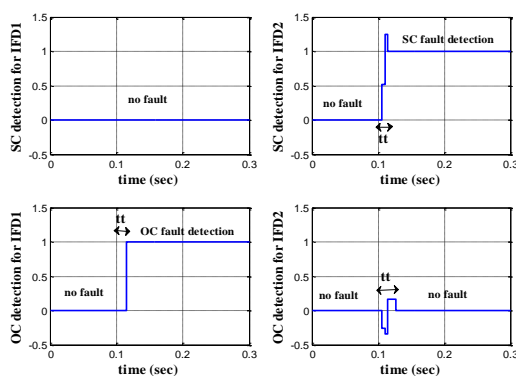


Fig. 39. Fault type identification for OC-Side1 and SC-Side2 (by neural networks)

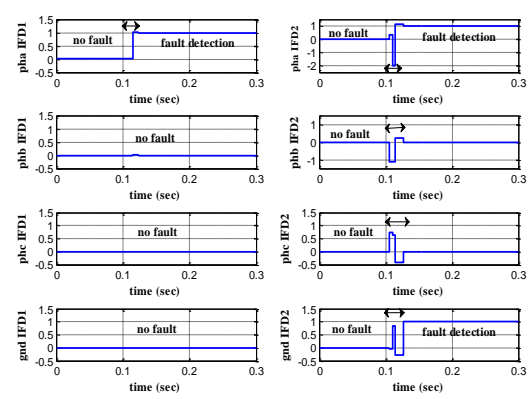


Fig. 40. Fault phase identification  $Ph_a$ -GND-Side2 (by neural networks)

Figures 41-48 show the diagnosis results of each IFD when applying a single-phase open circuit fault OC in  $Ph_a$ . Figures 41 and 42 indicate simple disturbances of voltages followed by a stability towards the initial values and a cancellation of the currents of phase (a) in both sides due to the opening of the power line.

The fuzzy logic was able to signal a fault in zone 1 with respect to side 1 (Fig. 43) and to identify the opening of phase a (Fig. 44 and 45).

The neural network also was able to signal and identify the same characteristics as fuzzy logic (Figs 46, 47 and 48): A line opening fault on zone 1 and on phase (a).

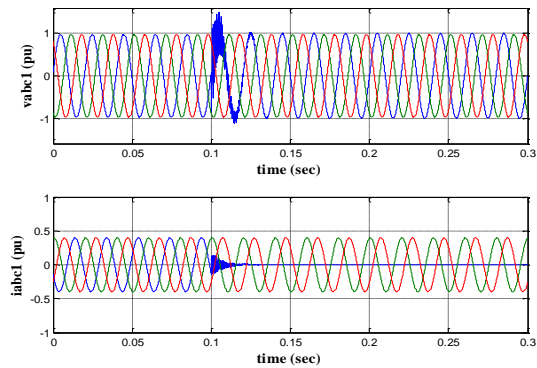


Fig. 41.  $V_{abc1}$  and  $I_{abc1}$  with OC fault of  $Ph_a$

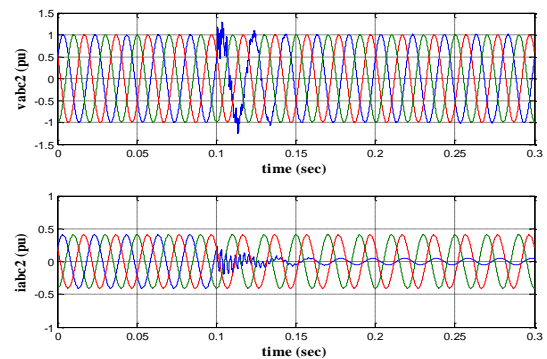


Fig. 42.  $V_{abc2}$  and  $I_{abc2}$  with OC fault of  $Ph_a$

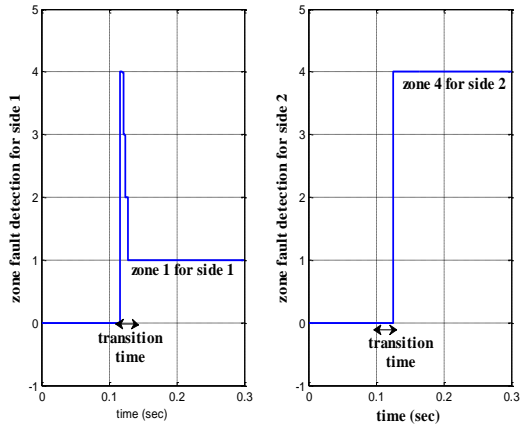


Fig. 43. Fault zone detection for OC Ph<sub>a</sub> (by fuzzy logic)

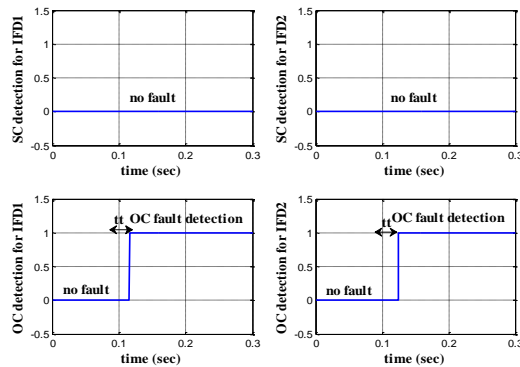


Fig. 44. Fault type identification for OC-Side1 and OC-Side2 (by fuzzy logic)

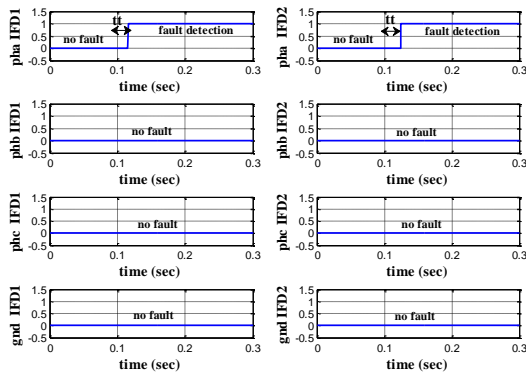


Fig. 45. Fault phase identification Ph<sub>a</sub> (by fuzzy logic)

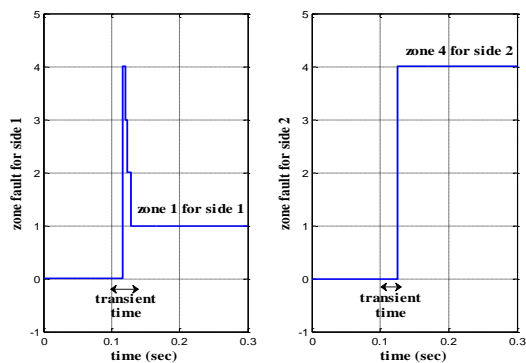


Fig. 46. Fault zone detection for OC Ph<sub>a</sub> (by neural networks)

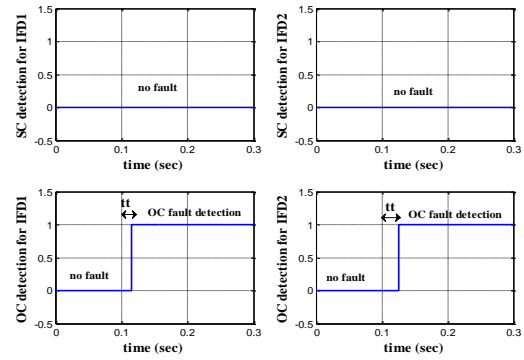


Fig. 47. Fault type identification for OC-Side1 and OC-Side2 (by neural networks)

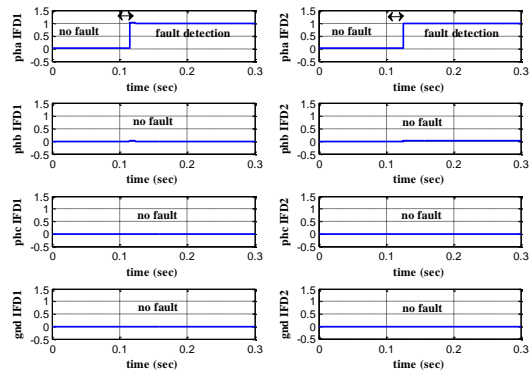


Fig. 48. Fault phase identification Ph<sub>a</sub> (by neural networks)

In this case a two phase short circuit to ground fault (LL-G) is applied in zone 2 on both sides: Figures 49 and 50 show a decrease in voltage of two phases (a) and (b) in the two sides of the test network (line), and consequently the increase in current in the two phases (a) and (b) because of SC.

The fuzzy logic was able to identify the correct fault zone; such as zone 2 in point of view of side 1 system and zone 3 in point of view of side 2 system. The fault type identification is also found in both sides as a SC short circuit on both phases (a) and (b). Always transient conditions after the fault has been introduced but within very short delays (20 ms) compared to the tripping time of the protection circuit breaker 200 ms (Figs. 51, 52, 53).

In the same way as fuzzy logic, the neural network was capable to obtain approximately the same performance of localization and identification. The important transient regimes are remarkable in comparison with fuzzy logic, after the occurrence of the fault.

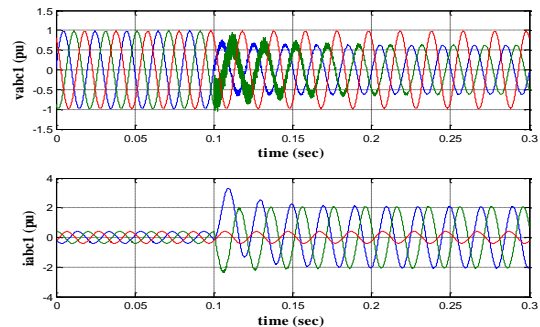


Fig. 49.  $v_{abc1}$  and  $i_{abc1}$  with SC fault of Ph<sub>a</sub>-Ph<sub>b</sub>-GND

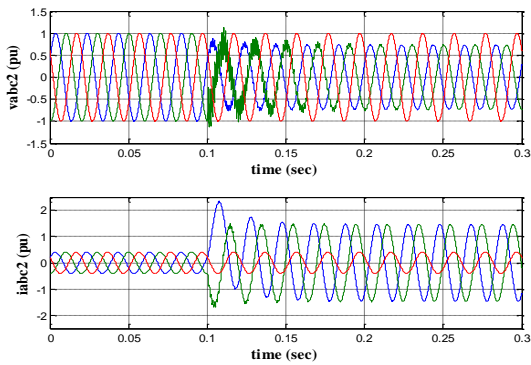


Fig. 50.  $v_{abc2}$  and  $i_{abc2}$  with SC fault of Ph<sub>a</sub>-Ph<sub>b</sub>-GND

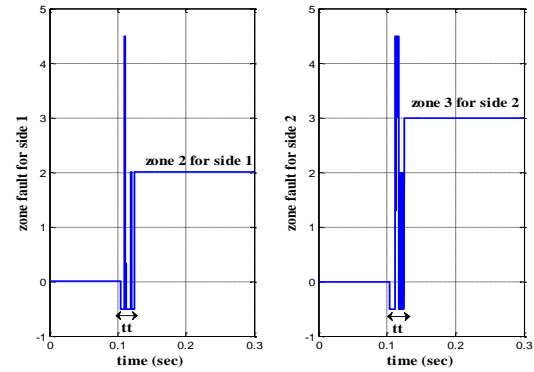


Fig. 54. Fault zone detection for SC Ph<sub>a</sub>-Ph<sub>b</sub>-GND (by neural networks)

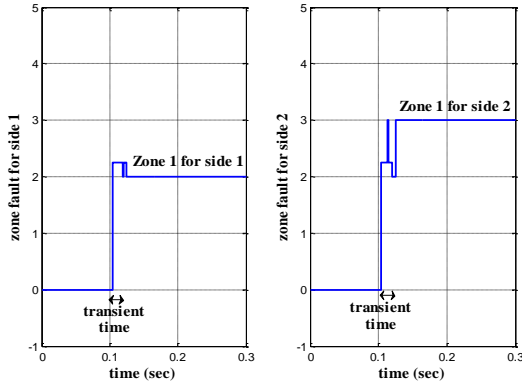


Fig. 51. Fault zone detection for SC Ph<sub>a</sub>-Ph<sub>b</sub>-GND (by fuzzy logic)

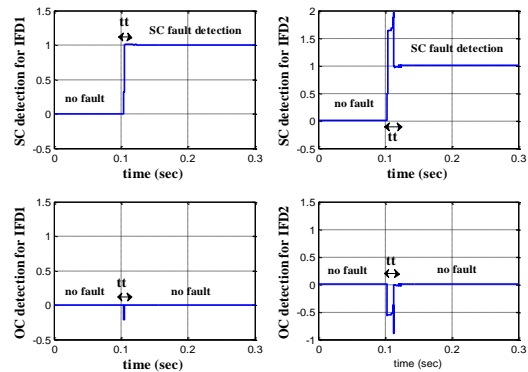


Fig. 55. Fault type identification for SC-Side1 and SC-Side2 (by neural networks)

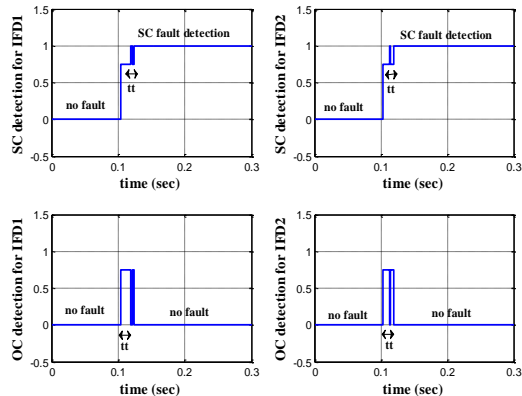


Fig. 52. Fault type identification for SC-Side1 and SC-Side2 (by fuzzy logic)

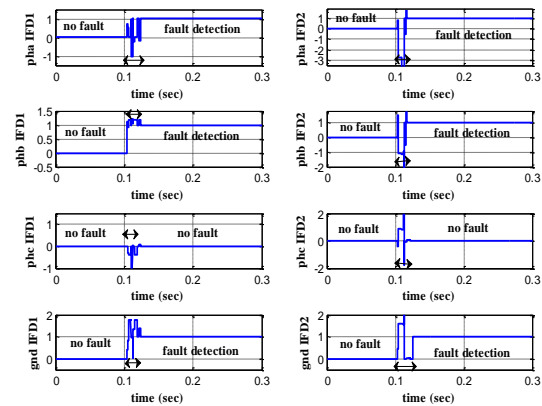


Fig. 56. Fault phase identification Ph<sub>a</sub>-Ph<sub>b</sub>-GND (by neural networks)

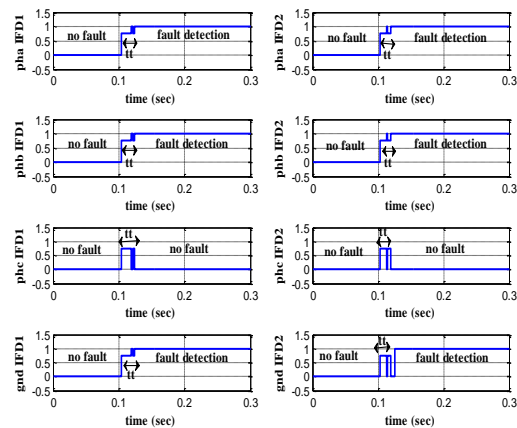


Fig. 53. Fault phase identification Ph<sub>a</sub>-Ph<sub>b</sub>-GND (by fuzzy logic)

As the same as previous case (two-phase ground (LL-G) fault), applying the same type of fault with a displacement by 15 km towards side 2 (zone2). The characteristics show practically the same electrical signal variations with slight decrease in currents (in SC fault phases). Regarding the detection, localization and fault identification performance for both diagnostic strategies (fuzzy logic and the neural network) the same results are obtained compared to the previous case (Figs. 57, 58, 59, 60, 61, 62, 63 and 64).

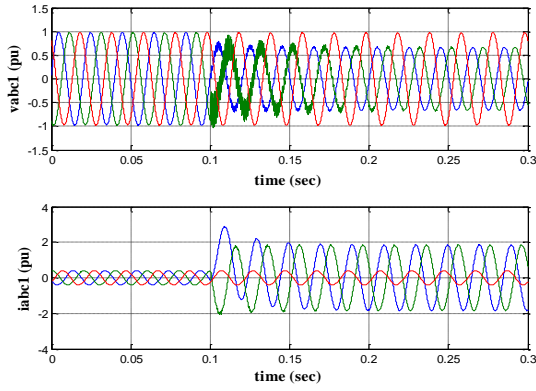


Fig. 57.  $v_{abc1}$  and  $i_{abc1}$  with SC fault of  $Ph_a-Ph_b-GND$  (Fault displacement at 15 km)

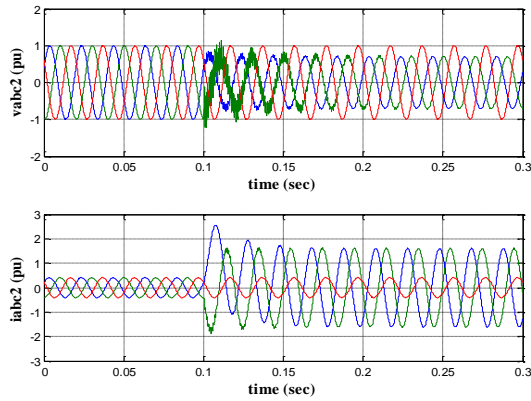


Fig. 58.  $v_{abc2}$  and  $i_{abc2}$  with SC fault of  $Ph_a-Ph_b-GND$  (Fault displacement at 15 km)

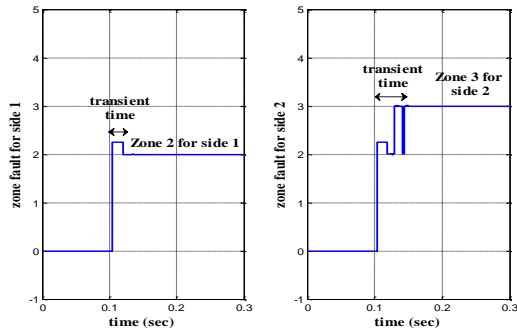


Fig. 59. Fault zone detection for SC  $Ph_a-Ph_b-GND$  (by fuzzy logic) : Fault displacement at 15 km

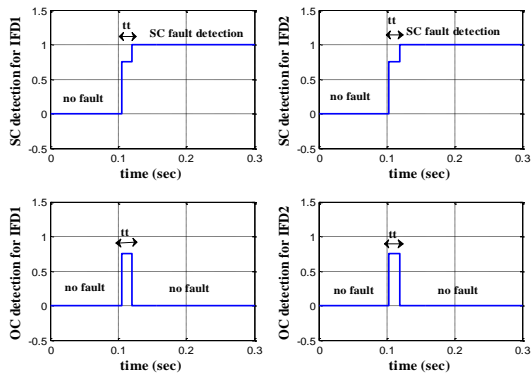


Fig. 60. Fault type identification for SC-Side1 and SC-Side2 (by fuzzy logic): Fault displacement at 15 km

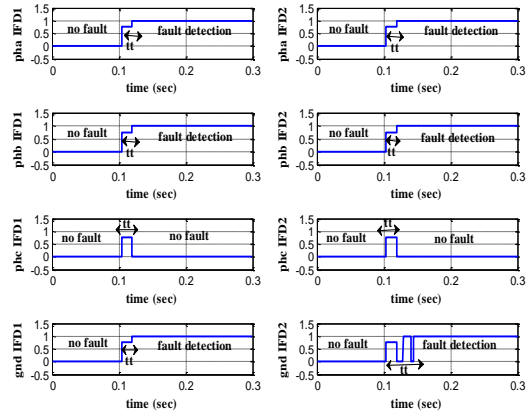


Fig. 61. Fault phase identification for  $Ph_a-Ph_b-GND$ : Fault displacement at 15 km (by fuzzy logic)

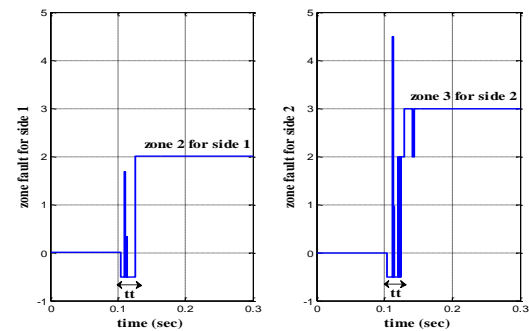


Fig. 62. Fault zone detection for SC  $Ph_a-Ph_b-GND$  (by neural networks): Fault displacement at 15 km

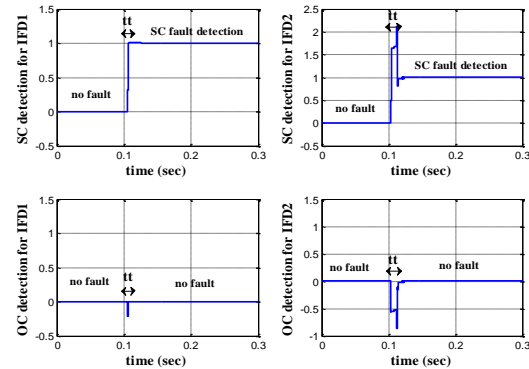


Fig. 63. Fault type identification for SC-Side1 and SC-Side2 (by neural networks): Fault displacement at 15 km.

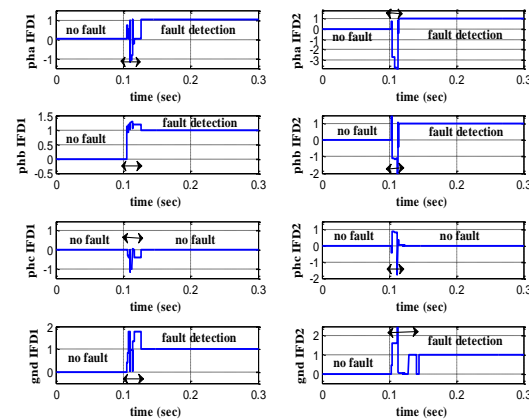


Fig. 64. Fault phase identification  $Ph_a-Ph_b-GND$  (by neural networks): Fault displacement at 15 km

To test the effectiveness of the diagnostic system in several fault variants, a two-phase short-circuit fault isolated from ground on zone 3 is studied in this case: The short circuit fault between the two phases (a) and (b): (The drop phase (a) on phase (b)). This type of fault allows an imbalance between the three phase's voltage and the three phase's current in the two sides of networks (Figs. 65, 66). The fuzzy logic algorithm was able to locate the SC fault correctly in zone 3 with respect to side 1 and zone 2 with respect to side 2. This method also is able to signal the fault on both phases (a) and (b). Likewise, the neural network is capable of detecting the SC fault on the two phases (a) and (b) in zone 3 compared to side 1 as shown in figures 70, 71 and 72.

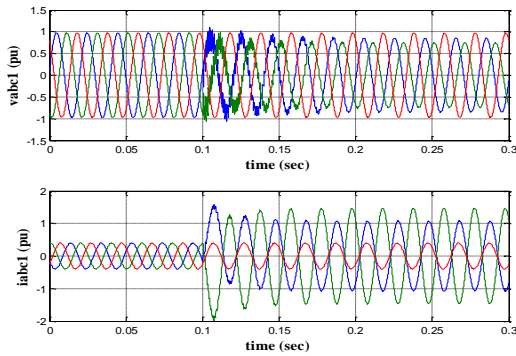


Fig. 65.  $v_{abc1}$  and  $i_{abc1}$  with SC fault of  $Ph_a-Ph_b$

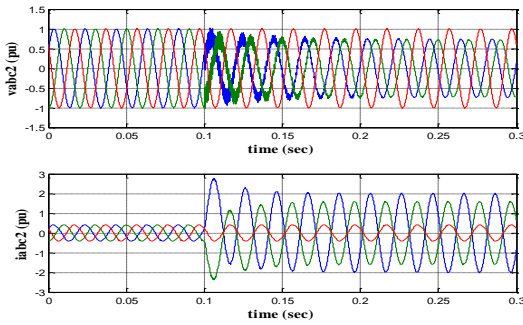


Fig. 66.  $v_{abc2}$  and  $i_{abc2}$  with SC fault of  $Ph_a-Ph_b$

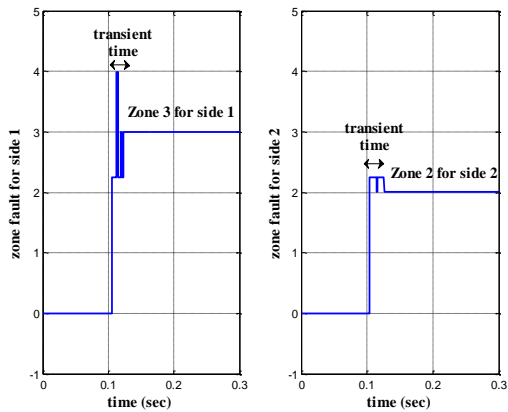


Fig. 67. Fault zone detection for SC  $Ph_a-Ph_b$  (by fuzzy logic)

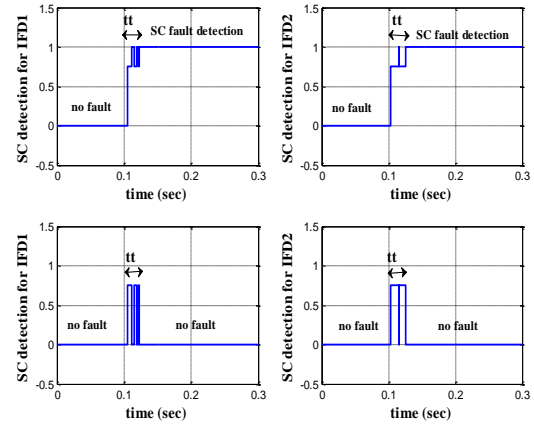


Fig. 68. Fault type identification for SC-Side1 and SC-Side2 (by fuzzy logic)

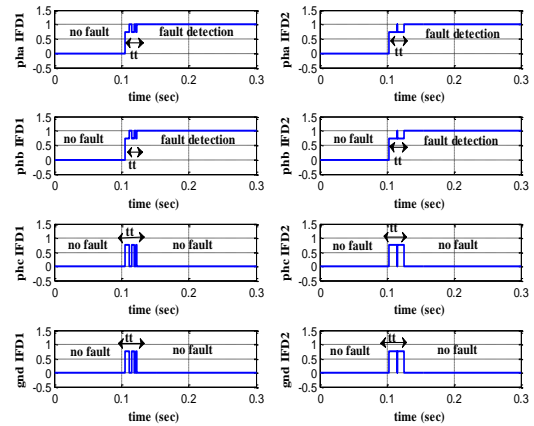


Fig. 69. Fault phase identification  $Ph_a-Ph_b$  (by fuzzy logic)

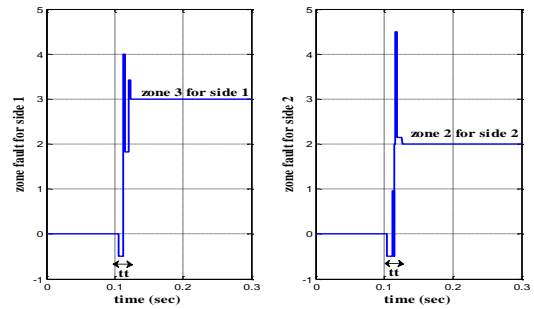


Fig. 70 . Fault zone detection for SC  $Ph_a-Ph_b$  (by neural networks)

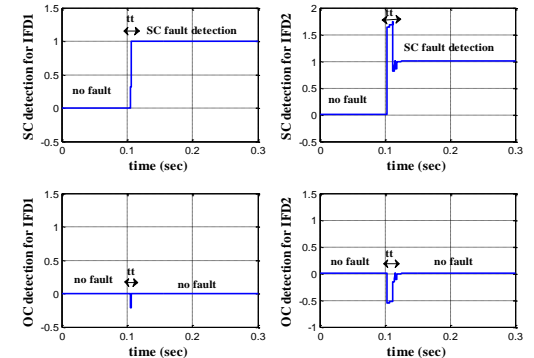


Fig. 71. Fault type identification for SC-Side1 and SC-Side2 (by neural networks)

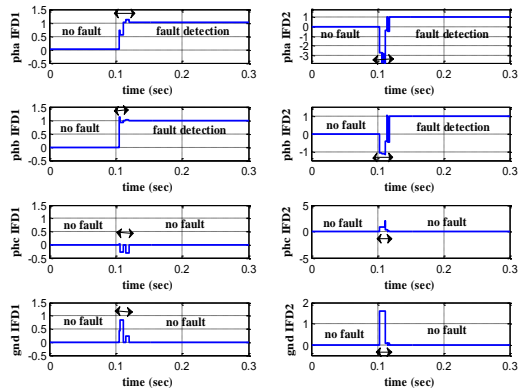


Fig. 72. Fault phase identification Ph<sub>a</sub>-Ph<sub>b</sub> (by neural networks)

**7.2. Robustness test**

To test the two strategies (fuzzy logic and the neural network) robustness, two tests are applied:

- Fault resistance variation (from 0Ω to 15Ω);
- Load variation: Variation of the voltage phase shift angle of source 2 (from 27° to 10°).

A single phase (LG) resistive SC ground fault is applied in zone 2 on side 1 (the same type of fault in section "7.1" but with a resistance of 15Ω). Figures 73 and 74 describe the variation in the electrical transient behavior (voltage-current) in the two sides of the test network: Practically, the same situation is obtained with the case of section "7.1": Where the fault resistance is zero. Despite the variation of the fault resistance from 0Ω to 15Ω, the fuzzy logic algorithm was able to signal the fault zone (Fig. 75), the type of fault (Fig. 76) and the identification of the phase of the fault (Fig. 77) correctly. The only difference is the considerable increase in the transient signaling and identification time after the fault occurrence. Also the neural network capable of reaching high signaling performance comparable to fuzzy logic with much lower transient delays compared to the breaker trip time (See Figures 78, 79 and 80).

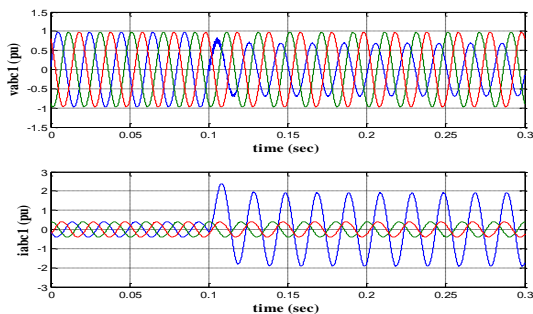


Fig. 73.  $v_{abc1}$  and  $i_{abc1}$  with SC fault of Ph<sub>a</sub>-GND-Side1: Fault resistance at 15 Ω

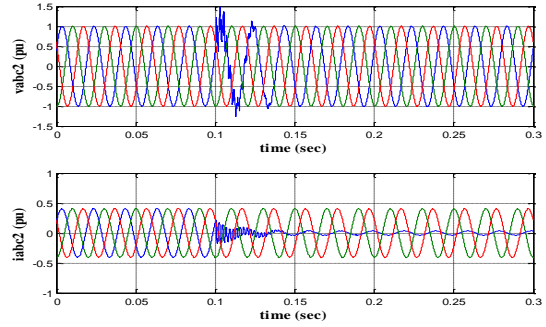


Fig. 74.  $v_{abc2}$  and  $i_{abc2}$  with SC fault of Ph<sub>a</sub>-GND-Side1: Fault resistance at 15 Ω

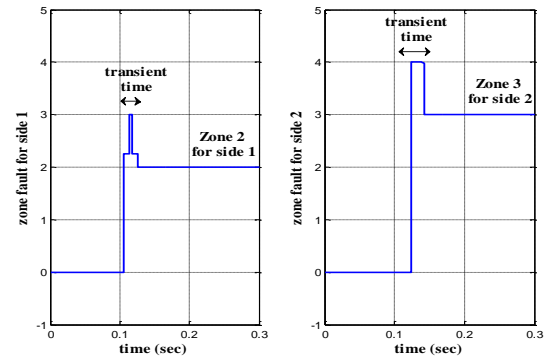


Fig. 75. Fault zone detection for SC Ph<sub>a</sub>-GND-Side1 (by fuzzy logic): Fault resistance at 15 Ω

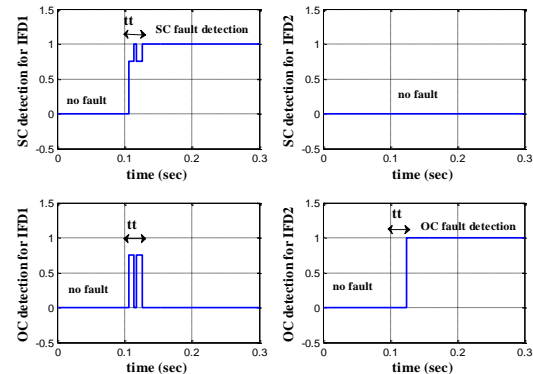


Fig. 76. Fault type identification for SC-Side1 and OC-Side2 (by fuzzy logic): Fault resistance at 15 Ω

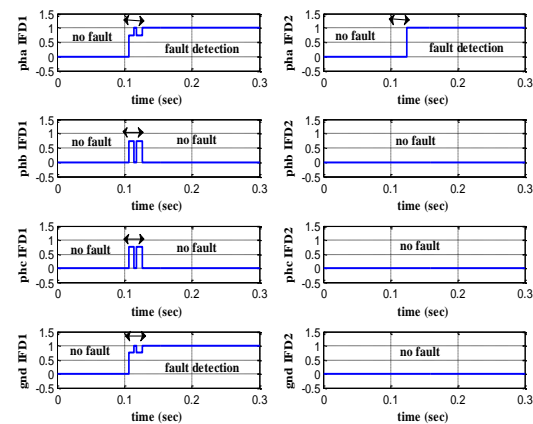


Fig. 77. Fault phase identification Ph<sub>a</sub>-GND-Side1 (by fuzzy logic): Fault resistance at 15 Ω.

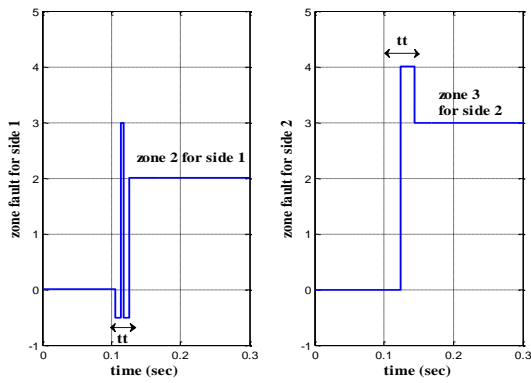


Fig. 78. Fault zone detection for SC Pha-GND-Side1 (by neural networks): Fault resistance at 15 Ω

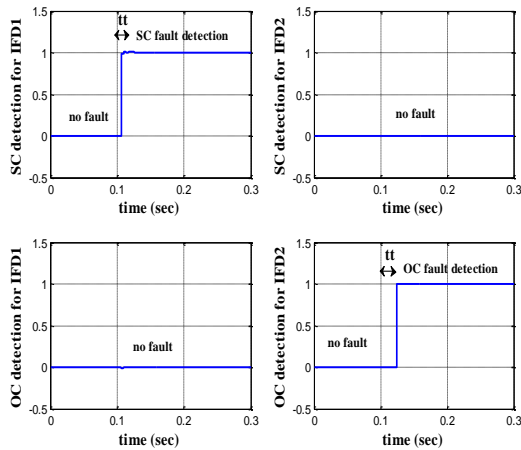


Fig. 79. Fault type identification Pha-GND-Side1 (by neural networks): Fault resistance at 15 Ω

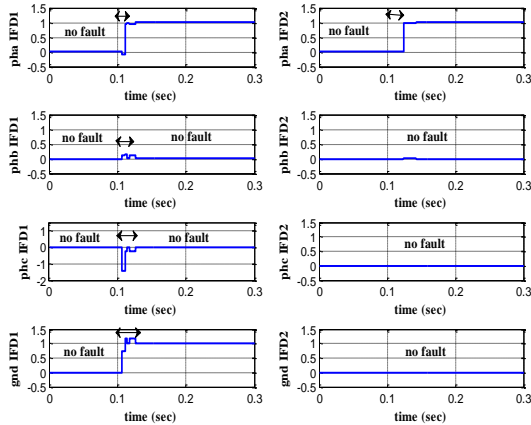


Fig. 80. Fault phase identification Pha-GND-Side1 (by neural networks): Fault resistance at 15 Ω

In this part an application of other disturbance in form of load variation or a variation in the power transmitted by the transmission line (by varying the voltage phase angle in source 2 from 27° to 10°) is analyzed. This disturbance causes the current increase and the voltage drop of phase (a) at side 1, and also the cancellation of the current of phase (a) without voltage change due to of the opening of the line at the fault point in side 2 (See figures 81 and 82).

Always fuzzy logic is able to identify all the fault characteristics with a significant increase in the transient signaling duration: This is the largest compared to all the previous cases, as shown in

figures 83, 84 and 85. Neural network signatures describe the same performances at the same transient durations compare to the fuzzy logic (See figures 86, 87 and 88).

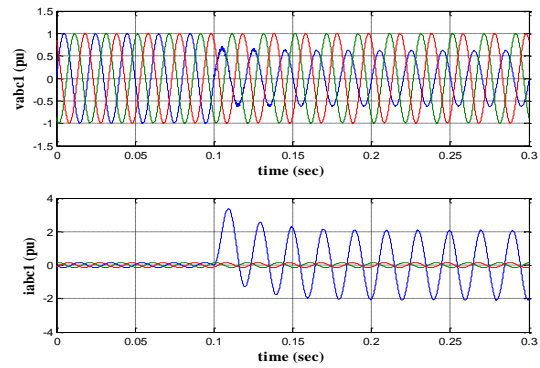


Fig. 81.  $v_{abc1}$  and  $i_{abc1}$  with SC fault of Pha-GND-Side1: For load variation

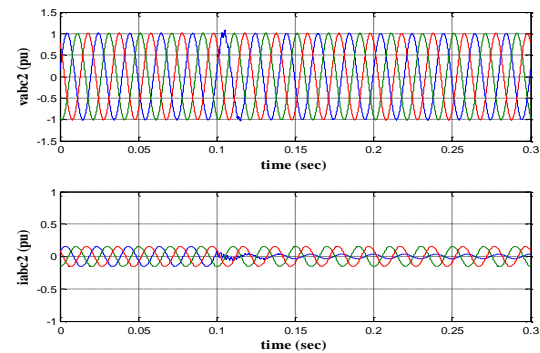


Fig. 82.  $v_{abc2}$  and  $i_{abc2}$  with SC fault of Pha-GND-Side1: For load variation

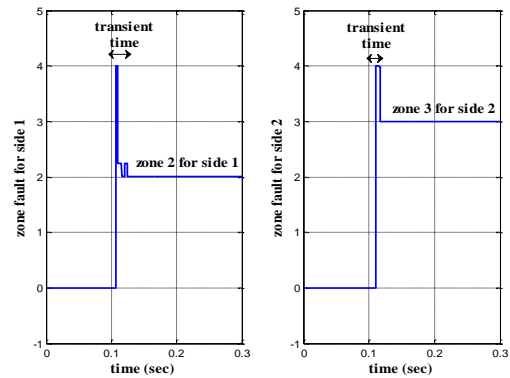


Fig. 83. Fault zone detection for SC Pha-GND-Side1 (by fuzzy logic): For load variation

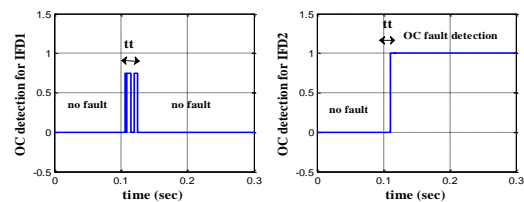
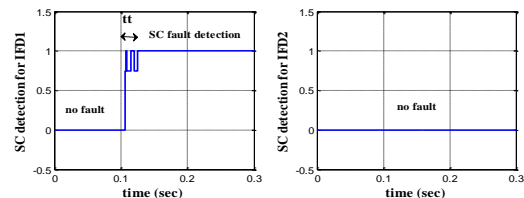


Fig. 84. Fault type identification for SC-Side1 and OC-Side2 (by fuzzy logic): For load variation

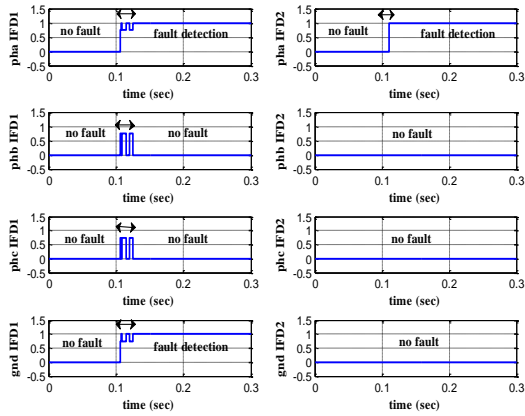


Fig. 85. Fault phase identification PhA-GND-Side1 (by fuzzy logic): For load variation

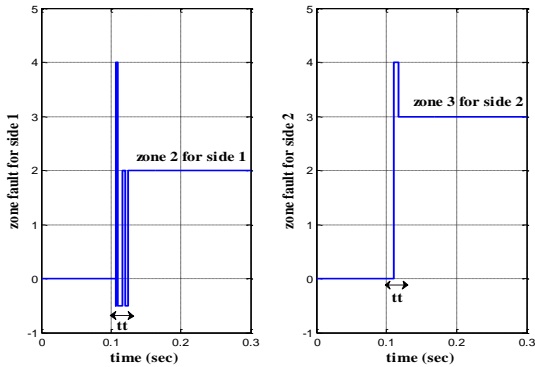


Fig. 86. Fault zone detection for SC PhA-GND-Side1 (by neural networks): For load variation

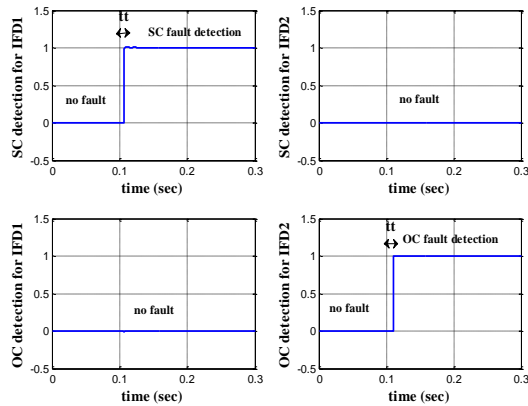


Fig. 87. Fault type identification for SC-Side1 and OC-Side2 (by neural networks): For load variation

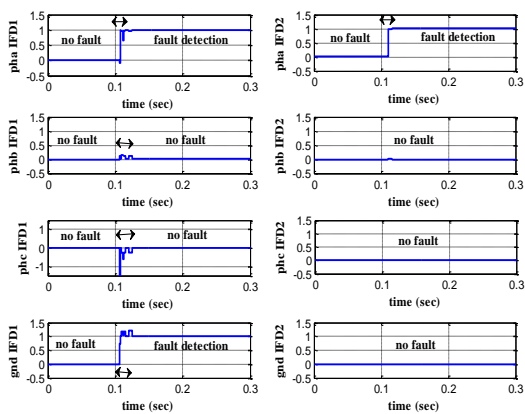


Fig. 88. Fault phase identification PhA-GND-Side1 (by neural networks): For load variation

## 8. CONCLUSION

This work proves the intelligent diagnosis by fuzzy logic and by the artificial neural network is a very efficient and very powerful solution for the monitoring of electrical transmission lines. Three-phase voltage and current signals were extracted from the measurements devices at both ends of the transmission line are used to synthesize these diagnostic systems, in which that the proposed methods eliminate the necessity of complex features extraction process and work directly on these signals amplitudes, this technique and the novel training strategy which uses a few training samples in form of intervals, thus having a great advantage of reducing the computational time and improving the performance.

The accuracy of both methods was evaluated by simulating a three-phase (230 kV, 50 Hz) transmission line with the length of 200 km. both methods were tested in different scenario such as different fault types, variations in fault resistance and in load phase angle.

In the execution of three tasks of detection, classification and localization of faults, the results were very promising indicating that both methods of them are reliable, fast (response time 20 ms which is shorter than the protection tripping time 200ms) and accurate (The fault zone is well determined when the fault occurs on the zone's boundaries and covers a large range of fault resistance) in addition.

This contribution also explains the technical obligation to integrate two diagnostic stations on the two power line terminals.

**Author contributions:** research concept and design, K.M.O.T., M.B., I.M., A.H.; Collection and/or assembly of data, K.M.O.T., M.B., I.M.; Data analysis and interpretation, K.M.O.T., M.B.; Writing the article, K.M.O.T., M.B., A.H.; Critical revision of the article, M.B., I.M., A.H.; Final approval of the article, M.B., A.H.

**Declaration of competing interest:** The authors declare that they have no known competing financial interests or personal relationships that could have appeared to influence the work reported in this paper.

## REFERENCES

1. Avagaddi P, Edward B, Ravi K. A review on fault classification methodologies in power transmission systems: Part-I. Journal of Electrical Systems and Information Technology. 2018;5(1):48-60. <https://doi.org/10.1016/j.jesit.2017.01.004>
2. Mukherjee A, Kundu P, Das A. Transmission Line Faults in Power System and the Different Algorithms for Identification, Classification and Localization: A Brief Review of Methods 2020.
3. Samantaray SR. A systematic fuzzy rule based approach for fault classification in transmission lines. Applied Soft Computing. 2013;13(2): 928-938. <https://doi.org/10.1016/j.asoc.2012.09.010>.
4. Di Santo SG, CEDM Pereira, Fault location method applied to transmission lines of general configuration. International Journal of Electrical Power & Energy

- Systems. 2015;69:287-294.  
<https://doi.org/10.1016/j.ijepes.2015.01.014>.
5. Ghorbani A, Sanaye-Pasand M, Mehrjerdi H. Accelerated distance protection for transmission lines based on accurate fault location. *Electric Power Systems Research*. 2021;193:107021  
<https://doi.org/10.1016/j.epsr.2021.107021>.
  6. Moravej Z, Pazoki M, Khederzadeh M. New smart fault locator in compensated line with UPFC. *International Journal of Electrical Power & Energy Systems*. 2017;92:125-135.  
<https://doi.org/10.1016/j.ijepes.2017.05.002>.
  7. Taheri R, Eslami M, Damchi Y. Single-end current-based algorithm for fault location in series capacitor compensated transmission lines. *International Journal of Electrical Power & Energy Systems*. 2020;123:106254. <https://doi.org/10.1016/j.ijepes.2020.106254>.
  8. Lopes F, Dantas K, Costa F. Accurate Two-Terminal Transmission Line Fault Location Using Traveling Waves. *IEEE Transactions on Power Delivery* 2018;33(2):873-880.  
<https://doi.org/10.1109/TPWRD.2017.2711262>.
  9. Parsi M, Crossley PA, Dragotti PL, Cole D. Wavelet based fault location on power transmission lines using real-world travelling wave data. *Electric Power Systems Research*. 2020;186:106261.  
<https://doi.org/10.1016/j.epsr.2020.106261>.
  10. Gonzalez-Sanchez VH, Torres-García V, and Guillen D. Fault location on transmission lines based on travelling waves using correlation and MODWT. *Electric Power Systems Research*. 2021;197:107308.  
<https://doi.org/10.1016/j.epsr.2021.107308>.
  11. Mamiş MS, Arkan M, Keleş C. Transmission lines fault location using transient signal spectrum. *International Journal of Electrical Power & Energy Systems*. 2013;53:714-718.  
<https://doi.org/10.1016/j.ijepes.2013.05.045>.
  12. Abd el-Ghany HA, Azmy AM, Abeid AM. A General Travelling-Wave-Based Scheme for Locating Simultaneous Faults in Transmission Lines. *IEEE Transactions on Power Delivery*. 2020;35(1):130-139.  
<https://doi.org/10.1109/TPWRD.2019.2931178>.
  13. Ding J, Wang X, Li L. Distributed Traveling-Wave-Based Fault-Location Algorithm Embedded in Multiterminal Transmission Lines. *IEEE Transactions on Power Delivery*. 2018; 33(6):3045-3054.  
<https://doi.org/10.1109/TPWRD.2018.2866634>.
  14. Akmaz D, Mamis MS, Arkan M, Tagluk ME. Transmission line fault location using traveling wave frequencies and extreme learning machine. *Electric power systems research*. 2018;155:1-7.  
<https://doi.org/10.1016/j.epsr.2017.09.019>.
  15. Naidu OD, Pradhan AK. A Traveling Wave-Based Fault Location Method Using Unsynchronized Current Measurements. *IEEE Transactions on Power Delivery*. 2019;34(2):505-513.  
<https://doi.org/10.1109/TPWRD.2018.2875598>.
  16. Ghazizadeh-Ahsaei M. Time-domain based fault location for series compensated transmission lines without requiring fault type. *Electric Power Systems Research*. 2020;181:106171.  
<https://doi.org/10.1016/j.epsr.2019.106171>.
  17. Saber A, Zeineldin HH, El-Fouly Thm, Al-Durra A. Time-Domain Fault Location Algorithm for Double-Circuit Transmission Lines Connected to Large Scale Wind Farms. *IEEE Access*. 2021; 9: 11393-11404.  
<https://doi.org/10.1109/ACCESS.2021.3049484>.
  18. Kumar BR, Mohapatra A, Chakrabarti S, Kumar A. Phase angle-based fault detection and classification for protection of transmission lines. *International Journal of Electrical Power & Energy Systems*. 2021;133:107258.  
<https://doi.org/10.1016/j.ijepes.2021.107258>.
  19. Ji L, Tao X, Fu Y, Fu Y. A New Single Ended Fault Location Method for Transmission Line Based on Positive Sequence Superimposed Network during Auto Reclosing. *IEEE Transactions on Power Delivery* 2019;34(3):1019-1029.  
<https://doi.org/10.1109/TPWRD.2019.2901835>.
  20. Fan R, Liu Y, Huang R, Diao R, Wang S. Precise Fault Location on Transmission Lines Using Ensemble Kalman Filter. *IEEE Transactions on Power Delivery*. 2018;33(6):3252-3255.  
<https://doi.org/10.1109/TPWRD.2018.2849879>.
  21. Shaik AG, Pulipaka RRV. A new wavelet based fault detection, classification and location in transmission lines. *International Journal of Electrical Power & Energy Systems*. 2015;64:35-40.  
<https://doi.org/10.1109/PECON.2006.346630>.
  22. Krishnanand KR, Dash PK, Naeem MH. Detection, classification and location of faults in power transmission lines. *International Journal of Electrical Power & Energy Systems*. 2015; 67:76-86.  
<https://doi.org/10.1016/j.ijepes.2014.11.012>.
  23. Han J, Miao S, Li Y, Yang W, Yin H. Faulted-Phase classification for transmission lines using gradient similarity visualization and cross-domain adaption-based convolutional neural network. *Electric Power Systems Research*. 2021;191:106876.  
<https://doi.org/10.1016/j.epsr.2020.106876>.
  24. Rafique F, Fu L, Mai R. End to end machine learning for fault detection and classification in power transmission lines. *Electric Power Systems Research* 2021;199: 107430.  
<https://doi.org/10.1016/j.epsr.2021.107430>.
  25. Chen K, Hu J, He J. Detection and Classification of Transmission Line Faults Based on Unsupervised Feature Learning and Convolutional Sparse Autoencoder. *IEEE Transactions on Smart Grid*. 2016;9:1748-1758.  
<https://doi.org/10.1109/TSG.2016.2598881>.
  26. Fathabadi H. Novel filter based ANN approach for short-circuit faults detection, classification and location in power transmission lines. *International Journal of Electrical Power & Energy Systems*. 2016; 74:374-383.  
<https://doi.org/10.1016/j.ijepes.2015.08.005>.
  27. Jiao Z, Wu R. A New Method to Improve Fault Location Accuracy in Transmission Line Based on Fuzzy Multi-Sensor Data Fusion. *IEEE Transactions Smart Grid*. 2019;10(4):4211-4220.  
<https://doi.org/10.1109/TSG.2018.2853678>.
  28. Wang T, Zhang G, Zhao J, He Z, Wang J, Pérez-Jiménez MJ. Fault Diagnosis of Electric Power Systems Based on Fuzzy Reasoning Spiking Neural P Systems. *IEEE Transactions on Power Systems*. 2015; 30(3):1182-1194.  
<https://doi.org/10.1109/TPWRS.2014.2347699>.
  29. Farshad M, Sadeh J. Accurate Single-Phase Fault-Location Method for Transmission Lines Based on K-Nearest Neighbor Algorithm Using One-End Voltage. *IEEE Transactions on Power Delivery*. 2012; 27(4): 2360-2367.  
<https://doi.org/10.1109/TPWRD.2012.2211898>.
  30. Safar H. Power transmission line analysis using exact, nominal  $\pi$ , and modified  $\pi$  models. in 2010 The 2nd International Conference on Computer and Automation Engineering (ICCAE) 2010.

31. Mohd Amiruddin AAA, Zabiri H, Taqvi SAA, Tufa LD. Neural network applications in fault diagnosis and detection: an overview of implementations in engineering-related systems. *Neural Computing and Applications*. 2020;32(2):447-472. <https://doi.org/10.1007/s00521-018-3911-5>.
32. Prakash S, Sinha S. Application of artificial intelligence in load frequency control of interconnected power system. *International Journal of Engineering, Science and Technology* 2011; 3. <https://doi.org/10.4314/ijest.v3i4.68558>.
33. Lv C, Yang X, Junzhi Z, Xiaoxiang N, Yutong L, Teng L, Dongpu C, Fei-Yue W. Levenberg–Marquardt Backpropagation Training of Multilayer Neural Networks for State Estimation of a Safety-Critical Cyber-Physical System. *IEEE Transactions on Industrial Informatics* 2018; 14(8):3436-3446. <https://doi.org/10.1109/TII.2017.2777460>.
34. Rubio JdJ. Stability Analysis of the Modified Levenberg–Marquardt Algorithm for the Artificial Neural Network Training. *IEEE Transactions on Neural Networks and Learning Systems* 2021; 32(8): 3510-3524. <https://doi.org/10.1109/TNNLS.2020.3015200>.
35. Thaker S, Nagori V. Analysis of Fuzzification Process in Fuzzy Expert System. *Procedia Computer Science*. 2018;132:1308-1316. <https://doi.org/10.1016/j.procs.2018.05.047>.

Received 2022-02-01

Accepted 2022-11-13

Available online 2022-11-14



**Khaled Omer Mokhtar TOUATI** was born in Djelfa Algeria on 26/05/1993. He received his license degree in 2014 and his master degree in 2016 in Electrical Engineering Specialization on Maintenance and Industrial Instrumentation

from Faculty of Science and Technology, University of Djelfa, Algeria . Now he is a PhD student in instrumentation and member in the Applied Automation and Industrial Diagnostics Laboratory, Faculty of Science and Technology, University of Djelfa, Algeria. His research interests include power system analysis.



**Mohamed BOUDIAF** received his Electrical Engineering Diploma in 2004 and Magister degree in 2007 from the Electrical Engineering Institute of The Ibn Khaldoun University, Tiaret, Algeria. From 2009 to 2020, He joined at the

Electrical Department, Ziane Achour University Djelfa. He received his Ph.D in June 2014 from the Electrical Engineering Department of The University of Sciences and Technology of Oran (USTO), Oran, Algeria. His research interests include power system analysis and FACTS devices.



**Imad MERZOUK**, was born in Mila, Algeria, in 1983. He received PhD of Science in Electrical Engineering degree in 2017 from the University of Batna, Algeria and the MSc. in Electrical Engineering degree in 2008 from the Polytechnics Military School (EMP), Algiers, Algeria, and the B.Sc. in Electrical Engineering degree in 2005 from the University of Jijel, Algeria. He is currently an associate professor at the department of Sciences and Technology, University of Djelfa, Algeria. His main fields of interests are control of power converters, power quality, and grid-connected renewable energy.



**Professor Ahmed HAFAlFA** was born in Algeria in 1974. He received the State Engineer degree in 2000 on Applied Automation, the Magister degree in 2004 on Applied Automation and control systems and the PhD on

Applied Automation and Signal Processing in 2010 from the UMBB Boumerdes University.

He received the Habilitation from the University of Sciences and Technology Houari Boumediene - USTHB - Faculty of Electronics and Computer Science, Department of Instrumentation and Automation on 2012. He is a PhD and Full Professor in Industrial Process: Automation / Diagnosis and Reliability Engineering at the Science and Technology Faculty of the University of Djelfa, Algeria, where he is pursuing his researches as a researcher at the Applied Automation and Industrial Diagnostic Laboratory of the University of Djelfa. Professor Ahmed HAFAlFA has participated in several international research projects and has led several national research projects. Currently he is the Director of the Applied Automation and Industrial Diagnostic Laboratory of the University of Djelfa. His research area of interests includes the modelling and control in industrial systems, the diagnosis and new reliability engineering, fault detection and isolation in industrials process, intelligent system based on fuzzy logic and neural networks.